

# Dalton Transactions

Accepted Manuscript



This is an *Accepted Manuscript*, which has been through the Royal Society of Chemistry peer review process and has been accepted for publication.

*Accepted Manuscripts* are published online shortly after acceptance, before technical editing, formatting and proof reading. Using this free service, authors can make their results available to the community, in citable form, before we publish the edited article. We will replace this *Accepted Manuscript* with the edited and formatted *Advance Article* as soon as it is available.

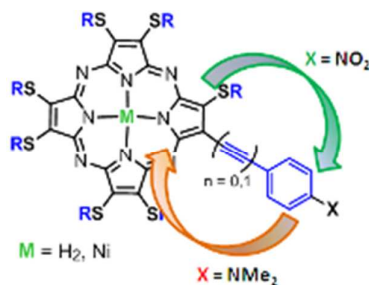
You can find more information about *Accepted Manuscripts* in the [Information for Authors](#).

Please note that technical editing may introduce minor changes to the text and/or graphics, which may alter content. The journal's standard [Terms & Conditions](#) and the [Ethical guidelines](#) still apply. In no event shall the Royal Society of Chemistry be held responsible for any errors or omissions in this *Accepted Manuscript* or any consequences arising from the use of any information it contains.

## Table of Contents Entry

### Non-symmetrical aryl- and arylolethynyl-substituted thioalkyl-porphyrazines for electronic materials: Synthesis, properties, and computational studies

Sandra Belviso\*, Mario Amati, Rocco Rossano, Alessandra Crispini and Francesco Leij\*



Porphyrazine ring shows ambivalent behavior, acting either as electron acceptor or electron donor in  $NMe_2$  or  $NO_2$  substituted compounds, respectively. Therefore, even this macrocycle mono-substitution provides an unconventional “push-pull” system.

# Non-symmetrical aryl- and arylethynyl-substituted thioalkyl-porphyrazines for electronic materials: Synthesis, properties, and computational studies

Sandra Belviso<sup>a,b\*</sup>, Mario Amati<sup>a,b</sup>, Rocco Rossano<sup>a</sup>, Alessandra Crispini<sup>c</sup> and Francesco Leij<sup>a,b\*</sup>

<sup>a</sup>*Università della Basilicata, Dipartimento di Scienze, via dell'Ateneo Lucano, 10; 85100 Potenza, ITALY.*

<sup>b</sup>*LASCAMM, CR-INSTM Unità della Basilicata and La.M.I.*

<sup>c</sup>*Centro di Eccellenza CEMIF.CAL-LASCAMM, CR-INSTM, Università della Calabria, Dipartimento di Chimica e Tecnologie Chimiche; 87026, Arcavacata di Rende (CS), ITALY.*

*Running title:* Non-symmetrical porphyrazines for electronic materials

*Keywords:* thio-porphyrazines, Suzuki coupling, Sonogashira coupling, non-linear optics, mesomorphism, organic photovoltaic.

Author to whom correspondence should be addressed:

Dr. Sandra Belviso  
Dipartimento di Scienze  
Università della Basilicata  
Via dell'Ateneo Lucano, 10  
I-85100 Potenza, ITALY  
fax: +39-0971-205678  
tel: +39-0971-205937  
e-mail: sandra.belviso@unibas.it

*Abstract*

A series of novel non-symmetrically substituted mono  $\beta$ -aryl and  $\beta$ -arylethynyl (alkylsulfanyl)porphyrazines and the corresponding Ni(II) complexes have been prepared by Suzuki-Miyaura and Sonogashira cross-coupling reactions with the aim to investigate substituent effects on their electronic and aggregation properties. Spectroscopic, electrochemical and computational investigations show that in both aryl and arylolethynyl compounds an efficient electron transfer between the aryl and macrocycle moieties occurs. The highest perturbation of the porphyrazine  $\pi$ -electron core is provided by strong electron-donating (NMe<sub>2</sub>) and electron withdrawing (NO<sub>2</sub>) aryl substituents, which increase and decrease the macrocycle electron density, respectively. Moreover, while in most of the compounds the LUMOs and HOMOs are mainly localized on the porphyrazine ring, in the amino-substituted derivatives the LUMO is localized on the peripheral aryl moieties and the HOMO on the macrocycle. Charge-transfer electronic excitations give rise to absorptions in UV-Vis spectra of both amino- and nitro-substituted compounds. In the former such excitations occur from aryl-localized to macrocycle-localized orbitals, while backward excitations occur in the latter. Therefore, the porphyrazine ring has an ambivalent behavior, acting as an electron acceptor in the case of the NMe<sub>2</sub>-substituted compounds and as an electron donor in the NO<sub>2</sub> substituted derivative. In these derivatives, even macrocycle mono-substitution provides unconventional “push-pull” systems suitable for NLO. Columnar discotic mesophases are also shown by thio-octyl arylolethynyl derivatives, allowing to envisage the possibility to achieve compounds both suitable for optoelectronic and endowed with self-aggregation properties.

## Introduction

Tetrapyrrole macrocycles, displaying highly delocalized  $\pi$ -electron systems, may provide an ideal structural framework from which to elaborate molecules with interesting non linear optical (NLO) properties,<sup>1</sup> a feature of prominent interest in the field of optical communications, information storage, optical switching, and electrooptical signal processing.<sup>2</sup> In particular, “push-pull” systems constituted by porphyrins<sup>3,4</sup> and phthalocyanines<sup>1-5</sup> non-symmetrically substituted at the periphery with suitable donor and acceptor (DA) groups exhibit second order nonlinear optical responses. Moreover, porphyrins and phthalocyanines with similar donor-bridge-acceptor structure constitute some of the most successful dyes employed in organic photovoltaic (OPV) devices.<sup>6</sup> In these systems the HOMO should reside on the donor portion while the LUMO is located on the acceptor portion and push-pull excitation creates an electron-hole pair at opposite sides of the molecule. Very recently, it has been also shown that porphyrin-based dyes substituted only with a donor moiety and lacking of a second acceptor unit, can still exhibit strong second harmonic generation (SHG).<sup>7</sup> In those “push-no-pull” systems the “free-base” porphyrins core is sufficiently electron-deficient to act as electron-acceptor. Such result indicates that the conventional push-pull design paradigm which guided till now the development of tetrapyrrole NLO dyes could be reconsidered and that the presence of an electron-accepting substituent could be not essential. The porphyrazine macrocycles,<sup>8</sup> structurally related to phthalocyanines, have been much less studied for optoelectronic applications. So far, only a few of these systems have been investigated for NLO applications<sup>9,10</sup> and no examples are reported for OPV devices. However, we expected that porphyrazine macrocycles singly-substituted with either donor or acceptor moieties could also constitute a “push-no-pull” system suitable for these applications. Therefore, we decided to synthesize new porphyrazines non-symmetrically substituted with either electron donor or acceptor moieties, in order to evaluate the influence of such moieties on molecular electronic and bulk properties relevant to second order NLO effects and possible applications in OPV. The synthesis of these compounds was approached starting from an advantageous preparative strategy to non-symmetrical (alkylsulfanyl)porphyrazines which we disclosed some years ago.<sup>11</sup> According to this procedure one alkylsulfanyl tail of a fully substituted porphyrazine, 2,3,7,8,12,13,17,18-octakis(alkylsulfanyl)-5,10,15,20-porphyrazine (H<sub>2</sub>OASPz) **1**, is replaced by a hydrogen atom, resulting in the non-symmetrically substituted 2,7,8,12,13,17,18-

heptakis(alkylsulfanyl)-5,10,15,20-porphyrzine (H<sub>2</sub>HASPz) **2** (Scheme 1). This approach paved the way to an easy access to non-symmetrically substituted porphyrzines, being the pyrrole β-hydrogen of **2** conveniently replaced by a bromine atom<sup>12</sup> leading to brominated intermediate **3** (Scheme 2) suitable for modulating non-symmetric peripheral substitution of the macrocycle. The synthetic potential of such strategy was then investigated to achieve peripheral substitution of non-symmetric porphyrzines with moieties able to modify both their charge distribution and molecular shape in order to tune their optical and electrical properties. Moreover, taking into account the growing interest in liquid-crystalline materials with NLO properties<sup>13,14</sup> and the importance of highly ordered columnar discotic self-assembled systems in photovoltaics,<sup>15</sup> we investigated also the effect of the peripheral substitution on the self-aggregation properties of these compounds. In fact, in previous studies we demonstrated that non-symmetric ‘free-base’ octylsulfanyl porphyrzine **2b** displays discotic mesomorphism,<sup>12</sup> unlike its symmetric counterpart **1b**.<sup>16</sup> The same behaviour is shown by its brominated derivative **3b**.<sup>12</sup> Probably, in these compounds, the permanent dipole induced by the non-symmetric shape of the macrocycle plays a role in stabilising ordered liquid crystalline phases,<sup>17</sup> a feature which might have relevance to the potential application of these discotic molecules in molecular electronics.<sup>13</sup> These mesomorphic properties were also retained by the corresponding Ni (II) complexes and by β-aryl substituted derivatives.<sup>18</sup> Therefore it can be envisaged the possibility to obtain non-symmetrically β-substituted porphyrzines with liquid-crystal (LC) behaviour for possible applications in NLO and photovoltaics. We then report herein the synthesis of a series of novel non-symmetrically substituted mono β-aryl and β-arylethynyl (alkylsulfanyl)porphyrzines and their Ni(II) complexes and a detailed experimental and computational study of their spectro-electrochemical and mesomorphic properties, with the aim to evaluate their potentiality in optoelectronics in future work.

## Results and Discussion

### *Synthesis*

In our previous studies on the synthesis and properties of thioalkylporphyrzines we set up a new preparative strategy (Scheme 1) to highly non-symmetric (alkylsulfanyl)porphyrzines

by hydrogen replacement of one alkylsulfanyl tail of the fully substituted porphyrazines **1**, resulting in the non-symmetrical  $\beta$ -H-substituted porphyrazines **2**.<sup>11</sup> Such approach displays the great advantage of a very clean reaction, easy purification procedures and yield larger than 40% of the desired non-symmetrically substituted products. The subsequent one-step replacement of the pyrrole  $\beta$ -hydrogen of **2** by a bromine atom leads to **3**, intermediates which allow the convenient introduction of different substituents on the macrocycle.<sup>12</sup> These easily accessible mono-bromo porphyrazines **3** are in fact suitable substrates on which substitution reactions can be carried out taking advantage of the numerous transition metal catalyzed cross-coupling reactions nowadays available in the synthetic armamentarium.<sup>19</sup> In order to tune both the molecular charge distribution and shape we turned out to arylation by Pd-catalysed Suzuki<sup>20</sup> coupling reactions,<sup>21</sup> and alkynylation by Sonogashira coupling<sup>22</sup> having access to the wide range of non-symmetric  $\beta$ -aryl and  $\beta$ -alkynyl substituted derivatives **5-12**. The use of palladium catalyzed couplings for the synthesis of functionalized tetrapyrroles has been widely explored in the case of porphyrins and phthalocyanines macrocycles,<sup>23</sup> while the first Suzuki cross-coupling arylation of porphyrazines has been already carried out by us in a preliminary investigation about the synthesis of mesomorphic (octylsulfanyl)porphyrazines.<sup>18</sup>

The non-symmetric porphyrazines **2a,b** were prepared from the parent symmetric 'free-base' **1a** and **1b** by treatment with the one-electron donor CrCl<sub>2</sub>, according to our already described procedure.<sup>12</sup> The latter were then brominated at room temperature in CHCl<sub>3</sub> with *N*-bromosuccinimide (NBS), affording **3a,b** in excellent (>90%) yield.<sup>12</sup> The arylated products **5-7** were then obtained in 15-25% yield from the brominated compounds **3a,b** by Suzuki cross-coupling. The coupling reaction was carried out heating at reflux in dry DMF/toluene (2:3, v/v) with excess (4 equiv) of the corresponding boronic acid, in the presence of excess of K<sub>2</sub>CO<sub>3</sub> and catalytic amounts of Pd(PPh<sub>3</sub>)<sub>4</sub> (10 % mol). Excess of the boronic acid was required to compensate for the competitive side reactions such as the hydrolytic deboration due to the presence of trace amounts of water.<sup>20,24</sup> In the case of 4-hydroxyphenylboronic acid these conditions did not provide the cross coupling reaction, therefore we turned out to employ the corresponding Ni-complex **4b**. In fact, as verified in our previous investigation,<sup>18</sup> the Suzuki coupling provides higher yields and faster reactions when performed on the Ni(II) complex compared to the corresponding 'free base' brominated heptakis-octylthio porphyrazines. The higher reactivity of the metal complexed macrocycles has been also

reported in the literature in the case of metal-catalyzed cross coupling on porphyrins.<sup>25</sup> In that case the ‘free bases’ porphyrins, although their electron deficiency should facilitate the carbon-halogen bond oxidative addition by the Pd catalysts,<sup>20</sup> react slower than the corresponding electron rich metal Zn(II) complexes. Interestingly, both DFT computations and <sup>13</sup>C NMR investigations allowed to ascertain that the presence of the metal does not significantly affect the electron density on the peripheral β-carbon atoms of the macrocycle, then excluding a role of Ni d orbitals on the molecular electronic and charge distribution (See discussion in ESI). Accordingly, **4b** was prepared by metalation of **3b** with NiCl<sub>2</sub>, then the cross coupling reaction of the Ni(II) complex **4b** with 4-hydroxyphenylboronic acid provided the desired arylated porphyrazine **12** in 25% yield. Finally, Ni-complex **8** was similarly achieved by metalation reaction of compound **7** with NiCl<sub>2</sub>. Following the Suzuki coupling approach we introduced aryl moieties that we expected to exert specific electronic effects on the macrocycles and then influencing their spectro-electrochemical properties. Therefore both electron withdrawing (CF<sub>3</sub>) and electron donating groups (OCF<sub>3</sub> and NMe<sub>2</sub>) were introduced on the phenyl moiety, as well as a hydrogen donor moiety like the OH.

Also the direct alkynylation of the “free-base” brominated compounds **3a,b** by Sonogashira coupling, did not provided the desired acetylenic derivatives, therefore it was necessary to carry out the coupling on the corresponding Ni(II) complexes **4a,b**, in turn obtained by Ni metalation of **3a,b**. As shown before for the Suzuki coupling, the Ni(II) complexes appear more reactive in Pd(0) catalysed cross-coupling reactions, probably giving rise to a faster oxidative addition step. Then, treatment of either **4a** or **4b** with 1.5 equiv. of the appropriate arylacetylene, in the presence of a catalytic amount of Pd(PPh<sub>3</sub>)<sub>2</sub>Cl<sub>2</sub> and CuI, with anhydrous triethylamine in THF provided β-arylethynyl (alkylsulfanyl)porphyrazines Ni(II) complexes **9-11** with yields in the 25-33% range after chromatographic purification.

### *Electrochemical study*

The electrochemical properties of the mono-substituted “free-base” and Ni-complexed porphyrazines **3-12** was investigated by cyclic voltammetry (CV) and differential pulse voltammetry (DPV). The electrochemical measurements were performed in CH<sub>2</sub>Cl<sub>2</sub> in the potential range -1.5 to 1.5 V (vs AgCl/Ag). The electrochemical results are gathered in Table 1 whereas Figure 1 shows the CV and DPV's of compound **8** as a typical representative of the series of compounds.

The redox behaviour of the studied compounds proved to be relatively simple. All the compounds showed, in the investigated cathodic region, two sequential one-electron reduction processes which can be assigned to the formation of a porphyrazine  $\pi$ -anion radical and a porphyrazine dianion, respectively.<sup>11,26,27</sup> These redox processes are characterized by a cathodic peak and its anodic counterpart displaying half-wave potentials,  $E_{1/2}$ , in the  $-0.8$  to  $-1.5$  V (vs Fc/Fc<sup>+</sup>) range. Both such processes can be considered as *quasi*-reversible because the conditions for the reversibility were not rigorously respected (see the values of the anodic vs cathodic current ratio,  $I_{pa}/I_{pc}$  and the separation of the oxidation and reduction peak potentials  $\Delta E_p = |E_a - E_c|$  from Table 1).

As inferred from Table 1 and Figure 2, a very good agreement among the CV and DPV reduction potentials was observed. The analysis of the electrochemical data for the ‘free-base’ porphyrazines **3a** and **5-7** pointed out that the introduction of a 4-phenylsubstituted moiety at the periphery of the macrocycle determines a cathodic shift of the reduction potentials. In fact, in respect to the Br-substituted porphyrazine **3a**, the 4-CF<sub>3</sub>Ph substituted compounds **5** showed a 5 mV more negative potential, while the 4-OCF<sub>3</sub>Ph derivative **6** displayed a 8 mV shift. A much larger cathodic shift (ca. 44 mV for the first reduction process) was observed when the phenyl moiety is *para*-substituted with the strong electron donating group NMe<sub>2</sub> (compound **7**). This suggests that the macrocyclic ring is the main responsible of the reduction process and that it is perturbed by the aryl substituent. In this sense, the phenyl moiety can permit an electron transfer between its *para*-substituent and the macrocyclic ring leading to the cathodic shift. It is in fact observed that electron-donating substituents such as NMe<sub>2</sub>, which should increase the electronic charge on the macrocycle, determine a more negative reduction potential, i.e. a more difficult reduction process. This phenomenon has been also observed in amino-porphyrazines in which the amino moiety is directly linked at the porphyrazine  $\beta$ -position.<sup>28</sup>

The substituent-induced trend in the reduction potentials is reproduced by our computations (see the “Computational Methods” section for details). As reported in Table 1 and showed in Figure 2, computations performed in-vacuum and in solution (by SCRF) reproduce the experimental trend in the series of the studied compounds. This suggests that the experimental trend can be associated to the intrinsic properties of the studied

compounds rather than particular solvation and/or aggregation phenomena in solution or at the surface of the working electrode.

As already observed in non symmetrically substituted porphyrzine **2a**<sup>11</sup> the introduction of Ni(II) into the macrocycle cavity, determines a significant cathodic shift of the reduction potentials. In fact, the first reduction potential of the Ni complex **4a** is 135 mV more negative than that of its ‘free-base’ counterpart **3a** and for the Ni complex **8** is 143 mV cathodic shifted in respect to its parent porphyrzine **7**. Also in this case, the computational analysis *in vacuo* (Table 1 and Figure 2) reproduces the experimental shifts and consequently suggests that metal-macrocycle interactions rather than environmental or aggregation effects are responsible of such behaviour. Figure 3 shows selected Kohn-Sham orbitals energy levels which are close to the HOMO and LUMO. The couple of close-in-energy virtual Kohn-Sham orbitals, LUMO and LUMO+1, are showed for **2** and **7**. Their composition in term of atomic orbital contributions is similar in all the studied compounds and the LUMO’s are mainly localised on the porphyrzine ring confirming that the reduction process predominantly involves the macrocycle.

A conformational analysis from the computed geometries shows that the phenyl ring in **5**, **6**, **7**, **8** and **12** does not lie in the same plane of the porphyrzine moiety. The dihedral angle between the average planes of the phenyl ring (C<sub>6</sub>H<sub>4</sub> fragment) and the macrocycle fragment (with the central metal when present but excluding the thioalkyl chains) spans the 35.9-39.0 degrees range with the lowest limit in **8** and the highest in **5** (see Figure S27 in ESI). According to our study, such torsional distortion does not impair the electronic delocalization between the substituent and the porphyrzine macrocycle. Table S2 and Figure S27 in ESI collect the macrocycle Mulliken charges (sum of Mulliken atomic charges) in the studied compounds. It can be noted that the computed porphyrzine moiety charge in **7** and **8** is significantly more negative compared to the other aryl-substituted compounds. Interestingly, an almost linear correlation between the phenyl-macrocycle dihedral angle and phenyl-to-macrocycle charge donation has been found in the five free-bases discussed here (see Figure S28 in ESI).

Several alkynyl-aryl substituted porphyrzines have been also prepared in order to move farther apart the aryl group from the macrocycle, so to induce coplanarity of the two moieties and to understand the influence of a “spacer” on the electron delocalization between the two aromatic units. In fact the alkynyl substituent though increasing the gap between the phenyl moieties and the macrocycle should preserve a significant electronic

coupling between them.-As observed above for the phenyl-substituted compounds, also in the Ni-complex **11** the presence of an electron-donating group like NMe<sub>2</sub> determines a cathodic shift (ca. 27 mV for the first reduction process) with respect to the unsubstituted parent compound **9a**, whereas the presence of the NO<sub>2</sub> electron-withdrawing group in **10** leads to an anodic shift of the potentials (ca. 58 mV for the first reduction process). Such a shift, induced by either electron donating or electron withdrawing substitution, has been also observed in symmetrically substituted tetrakis(arylethynyl) porphyrins.<sup>29</sup> By comparing the two -NMe<sub>2</sub> substituted Ni-complexes **8** and **11**, it is worth note that the effect of the electron-releasing group on the macrocycle is similar in both cases and, according to CV and DPV measurements, it is more significant in the case of **8** (higher experimental LUMO energy in Table 1). Computational results suggest that environmental effects play a certain role in the electrochemical behaviour. In fact, in case of these two compounds computations taking into account solvent effects, though by means of a continuum reaction field, correctly reproduce the experimental trend, whereas those *in vacuuum* display a reverse order. The same computations (see Figure S27 and Table S2 in ESI) revealed that larger charge transfer takes place in **11**, suggesting that the increased planarity could effectively improve the electronic conjugation between the substituent and the rest of the molecule. Furthermore CV of compounds **3a**, **5-8** exhibited a *quasi*-reversible oxidation wave at the upper limit of the anodic region, with  $E_{1/2}$  in the 0.3 to 0.7 V (*vs* Fc/Fc<sup>+</sup>) range, while alkynyl-substituted complexes **9a**, **10**, **11** showed an irreversible wave with a peak potential ( $E_p$ ) in the 0.3-0.7 V (*vs* Fc/Fc<sup>+</sup>) range. For compounds **4a** and **12** the oxidation process was clearly detected only by DPV experiment. In agreement with reduction data, but in a more definite way, the NMe<sub>2</sub> substituted compounds **7**, **8**, and **11** appear to be more easily oxidized than the other compounds and, among them, Ni-complex **8** is oxidized easier than the associated 'free-base' **7**. The DFT calculations indicate that in the three compounds the HOMO is mainly localized on the dimethylamino substituted phenyl ring. In the other studied cases, it is mainly localized on the macrocycle. Figure 3 shows the change in the HOMO localization in selected compounds. Therefore, in the presence of NMe<sub>2</sub> substituents, the oxidation mainly involves the aryl moiety, whereas, in all the other cases, it takes place on the porphyrazine core. For this reason, as far as oxidation potentials are concerned, amino substituted compounds cannot be directly compared with the other differently substituted derivatives. However, a comparison can be made between the ethynylphenyl substituted

Ni-complexes **9a** and **10**, from which it emerges that the electron withdrawing NO<sub>2</sub> group decreases the tendency to oxidation of the macrocycle and its net charge as well, inducing an anodic shift of the potential.

Finally, a comparison between the two unsubstituted ethynylphenyl Ni-complexes **9a** and **9b** having peripheral ethyl and octyl alkyl chains, respectively, shows a chains length effect on the potential values. It was observed, in particular, that the longer the peripheral alkyl chains the more cathodic are the potential values of the two reduction waves and more anodic is the potential value of the oxidation process. The same trends can be observed when *in-vacuo* computations are compared with the solution ones; as easily expected, the lack of a polarizable environment makes more difficult the oxidation and reduction process. This could suggest that the longer alkyl chains induce a less polarizable environment outside the porphyrazine ring, a fact that has been already reported.<sup>11,12</sup> Remarkably, all the studied compounds display HOMO levels lower than -5.2 eV and HOMO-LUMO bandgaps in the 1.3-1.8 range which make these aryl-substituted porphyrazines possible ideal candidates for [6,6]-phenyl-C61-butyric acid methyl ester (PCBM) based organic photovoltaic (OPV) devices.<sup>30</sup>

### *Spectroscopy*

The substituent effect on the optical properties of the studied non-symmetric ‘free-base’ porphyrazines **3a,5-7** was investigated by UV-Vis absorption spectroscopy (Table S1 in ESI), comparing their main spectral features with those of the parent unsubstituted non-symmetric ‘free-base’ porphyrazine **2a**. As previously reported, the latter, like its symmetrically substituted counterpart **1a**, shows an intense  $\pi \rightarrow \pi^*$  band at  $\approx 350$  nm (the B or Soret band), two almost equally intense  $\pi \rightarrow \pi^*$  bands at 636 and 704 nm (Q bands) and an additional, rather intense absorption due to  $n_{\text{Sulfur}} \rightarrow \pi^*$  transitions at 472 nm (“extra band”).<sup>11,31,32</sup>

The most conspicuous change in the optical spectra on going from the symmetric to the non-symmetric porphyrazines results in a generalized, although not homogeneous, blue shift in the range 400–700 nm. Actually, for **2a** the Q-band main peak lies 10 nm lower than in the case of its symmetrically substituted counterpart, and the broad band due to  $n_{\text{Sulfur}} \rightarrow \pi^*$  transitions is blue shifted 26 nm with respect to the corresponding band of **1a**. In fully substituted (alkylsulfanyl)porphyrazines the Q band wavelength is about 90 nm higher than for peripherally non substituted ‘free-base’ porphyrazines.<sup>33</sup> Therefore, the blue shift observed

in the spectrum of **2a** can be ascribed to the lack of one alkylsulfanyl moiety perturbing the porphyrazine  $\pi$  levels.

The optical spectrum ( $\text{CH}_2\text{Cl}_2$ ) of the non-symmetric brominated porphyrazine **3a** is almost superimposable with the one of the parent **2a**,<sup>11</sup> the only difference given by the strong (ca. 40 nm) red shift of the  $n_{\text{Sulfur}} \rightarrow \pi^*$  band which is now found at 511 nm. Such a red shift is less pronounced (ca. 25 nm) in the case of the porphyrazines **5** and **6** substituted with a phenyl moiety bearing both electron withdrawing  $\text{CF}_3$  and electron donating  $\text{OCF}_3$  groups (Figure 4). In these compounds such a band is in fact located around 495 nm. Interestingly, the substitution of the phenyl moiety with a strong electron-releasing group, like the *N,N*-dimethylamino one in **7**, gives rise to an extra band at 511 nm, whose red shift (40 nm) in respect to **2a** was comparable with the one observed in **3a**. This band was however almost completely overlapped by another one, at 555 nm, which appeared like a shoulder of the 630 nm band (Figure 4 and Table S1 in ESI). Only compound **7** also showed a slight red shift of the lower energy Q band which moves from 704 to 713 nm.

More interestingly, in **7**, a tail of the most intense Q band is present which gives rise to absorption even at 800 nm (Figure 4). Computational investigations based on the TDDFT approach were addressed to give an explanation of such widening of the Q band in its red portion. In Figures 5a and 5b the experimental extra and Q bands are showed for **2a** and **7**. Here, because the linear relation to the energy,  $\text{cm}^{-1}$  rather than nm are used. According to the computations, the **2a** Q bands (Figure 5a) are the results of two intense electronic transitions toward  $S_1$  and  $S_2$ . They consist in macrocycle-localised  $\pi-\pi^*$  electronic excitations from the HOMO to the couple of almost degenerate LUMO and LUMO+1 orbitals (see Figure 3 and 5a). Figure 5b shows that the Q bands have a more complex origin in **7**. In this case, excitation toward  $S_3$  and  $S_4$  correspond to the  $\pi-\pi^*$  transitions of **2a** ( $S_1$  and  $S_2$  in Figure 5a) and two new transitions appear ( $S_1$  and  $S_2$  in Figure 5b) whose nature is different. In fact, they are described as charge-transfer mono-electronic excitations from the HOMO now localised on the *N,N*-dimethylamino-phenyl fragment to the “couple” of macrocycle LUMOs (Figure 3 and 5b). The change in electronic structure in the case of **7** is confirmed by the voltammetric experiments. As indicated in Figures 2, 3 and Table 1, the presence of *N,N*-dimethylamino-phenyl structures in the non-symmetric substituent induces evident shifts of the oxidation peaks toward negative potentials which suggests a higher energy HOMO.

In the UV-Vis spectra ( $\text{CH}_2\text{Cl}_2$ ) of the Ni-complexes **4a** and **8** a single Q band is visible, due to their higher molecular symmetry, and the whole spectrum is blue shifted (ca. 30 nm),

compared to the corresponding ‘free-bases’ (Figure 6). Compared to the Br substituted compound **4a** the UV-Vis spectrum of the 4-NMe<sub>2</sub>Ph substituted nickel complex **8** shows a red shift (32 nm) and a widening of the extra band joined to a small bathochromic shift of the Q band, passing from 655 nm to 665 nm. As in compound **7**, absorption at 800 nm due to a Q band tail is present also in the spectrum of the 4-NMe<sub>2</sub>Ph substituted nickel complex **8**.

Figures 5c and 5d reports the **4a** and **8** low-energy parts spectra and their assignment according to the performed TDDFT computations. As in **2a** (Figure 5a), the **4a** Q band is described as the results of excitations toward S<sub>4</sub> and S<sub>5</sub> and, also in this case, they can be considered the same macrocycle-localised  $\pi$ - $\pi^*$  transitions (monoelectronic excitations from the HOMO to the LUMO and LUMO+1 in Figure 3). In **8**, relatively intense low-energy absorptions are originated (in particular the transition toward S<sub>1</sub> in Figure 5d) which can be considered the same charge transfer excitations from the *N,N*-dimethylamino-phenyl moiety to the macrocycle. In fact, they mainly consist in monoelectronic excitations from the HOMO to the LUMO and LUMO+1 but, also in this case, the HOMO is mainly localised on the *N,N*-dimethylamino-phenyl fragment (Figure 3). As observed in the case of tetrakis arylethynyl substituted porphyrins,<sup>29</sup> the bathochromic shift in **8** reflects an effective electronic delocalization between the porphyrazine core and the peripheral aryl groups. Moreover, the appearance of low-energy charge transfer transitions induced by the presence of the *N,N*-dimethylamino-phenyl substituent makes these compounds possible candidates for application in non-linear optics.<sup>7,34</sup>

The UV-Vis spectra (CH<sub>2</sub>Cl<sub>2</sub>) of the Ni-complexes **9a**, **10**, **11** in which a triple bond was introduced between the porphyrazine and the aryl moieties were then analyzed and compared with the Br substituted Ni-complex **4a** (Figure 6 and Table S1 in ESI) In all the acetylenic derivatives a bathochromic shift of the extra and Q bands in respect to **4a** was observed. The spectrum of the *N,N*-dimethylamino substituted phenylacetylene compound **11** is nearly superimposable with the one of the corresponding 4-NMe<sub>2</sub>Ph substituted derivative **8**. Apparently the introduction of the triple bond does not influence (as far as the optical properties are concerned) the electronic interaction between the aza-macrocycle and the phenyl-substituted moiety. This result is important because it shows that the introduction of the acetylenic spacer allows to modify the geometrical properties of the molecule, retaining the electronic interaction observed in the simplest aryl substituted derivative **8**.

The UV-Vis spectra of compounds **9a** and **10** are almost coincident with the one of compound **4a** except for an additional shoulder of the Soret band at 376 nm (26250 cm<sup>-1</sup>) visible in the

case of the nitro compound **10** and a higher general absorptivity in the region between the extra band and the onset of the Soret band. Such features are visible in Figures 6 and 7 which compares the two experimental spectra in this region.

In **9a** (Figure 7a), the extra band is mainly associated to excited states  $S_{12}$  and  $S_{14}$ . At higher wavenumbers no strong absorption intensities are computed up to about  $27000\text{ cm}^{-1}$ , where the Soret band begins. A different behaviour was observed for **10** and reported in Figure 7b. Also in this case,  $S_{12}$  and  $S_{14}$  are mainly associated to the extra band but an intense transition, not present in **9a**, is now computed at  $24597\text{ cm}^{-1}$  and associated to  $S_{22}$ . Such transition justifies the higher absorptivity of **10** in this energy range and, possibly, the shoulder of the Soret band.

According to our computations,  $S_{22}$  in **10** has a definite multideterminal composition and the most important contributions (Figure 8) involve excitations from HOMO-4 to HOMO-1 (orbital 211 to 214) as starting orbital and, interestingly, only the LUMO+2 (virtual orbital 218) as end orbital. In this light, from the orbital composition in Figure 8, it can be considered a combination of both a charge transfer from the macrocycle to the nitrophenyl substituent and, in part, a charge transfer within the porphyrazine substituent (from the triple bond to the nitrophenyl group). In **9a** (and in the other studied porphyrazines), the analogous (in terms of atomic orbital composition) of the 218 orbital is the orbital 209 (Figure 8) that lies at much higher energy because of the lack of the high electronegativity action of nitro group. For this reason, transitions involving this orbital move at higher energies and are not visible in the energy range between the extra and Soret bands. Comparing the UV-Vis spectrum in  $\text{CH}_2\text{Cl}_2$  of compound **9a** with that of **9b**, the effect of the increased length of the peripheral chains in **9b** consists in a slight red shift (ca. 10 nm) of the  $n_{\text{Sulfur}} \rightarrow \pi^*$  band.

The UV-Vis spectra of compounds **3a-11** were recorded also in toluene, in order to reveal the possible presence of solvatochromism effects (Table S1 in ESI). For all the studied compounds a lowering of the Soret band intensity is observed. The most significant solvatochromic effects are observed in the case of the bromo substituted compound **3a** which in toluene shows the  $n_{\text{Sulfur}} \rightarrow \pi^*$  band widened and split into two components at 502 and 544 nm, respectively (Figure S1 in ESI). Concerning the phenyl substituted 'free-base', solvent effects are observed only in the case of the 4-NMe<sub>2</sub>Ph substituted derivative **7** in which the  $n_{\text{Sulfur}} \rightarrow \pi^*$  band and the high energy the Q band at 630 nm overlap each other given rise to a large absorption in toluene (Figure S2 in ESI). As far as the Ni-complexes are concerned the change from  $\text{CH}_2\text{Cl}_2$  to toluene influences only the spectrum of the Br derivative **4a** which

displays a ca. 10 nm red shift of the extra band and a 5 nm shift of the Q-band. We have performed further SCRF TDDFT computations using toluene as solvent. Compared to the CH<sub>2</sub>Cl<sub>2</sub> computations (Figure 5c), the 5 nm red-shift of the Q-band is well reproduced. This fact suggests that this solvatochromic behaviour is mainly associated to the change in solvent polarity. However, the experimental shift of the extra band was more difficult to justify possibly due to the complex nature of such band, which is described as resulting from the combination of several similarly intense transitions. Alternatively, it is possible to think that such a shift could be associated to solvent influences on molecular vibrations and/or changes in the preferred orientation of the thioalkylic lateral chains that go beyond the “simple” effect of the modification of the solvent dielectric properties on the electronic energies. In case of compound **10**, where the phenylacetylene is nitro substituted, the combination of a slight red shift and widening of the Soret band which determine the disappearance of the 376 nm shoulder is observed in toluene (Figure S3 in ESI). Also in this case, SCRF TDDFT computations in toluene indicate a 5 nm blue shift of the transition toward S<sub>22</sub> (Figure 7). Such transition was assigned to the Soret shoulder at longer wavelengths, thus the computed blue shift is a clue in favour of its merging with the Soret band. Such an overlap could concur to apparently broaden the same band and red-shift its maximum. Finally, it should be noted that for all the 4-*N,N*-dimethylaminophenyl substituted compounds **7**, **8**, **11** the weak absorption at longer wavelengths (around 800 nm) observed in CH<sub>2</sub>Cl<sub>2</sub> is removed in toluene. Such solvatochromic effects experimentally confirm the charge-transfer origin of both the Soret low-energy shoulder in the nitro-derivative **10** and the high wavelengths Q band tail in amino-substituted **7**, **8**, **11**, in agreement with the computational investigation.

### *Mesomorphism*

To gain insight on the effect of peripheral substitution on the self-organizing capability of the non-symmetric porphyrazines in LC phases, in a previous study<sup>18</sup> we compared the mesomorphic behavior of the heptakis(octylsulfanyl)- $\beta$ -aryl substituted nickel compounds **14-15** with that of the parent compounds **2c** and **4b** (Chart). While compounds **2c** and **4b** showed a remarkable liquid-crystalline behaviour, displaying each two columnar mesophases and a very wide thermal stability  $\Delta T$  up to ca. 100°C ( $\Delta T = T_{\text{isotropization}} - T_{\text{melting}}$ ), phenyl substituted non-symmetric derivative **14** showed hexagonal columnar mesophases with low

isotropization temperature, which decrease  $\Delta T$  to 36.0°C. Moreover the 4-*N,N*-dimethylaminophenyl substituted derivative **15** did not show mesomorphic behavior at all.

In order to obtain non-symmetrically substituted porphyrazines with mesomorphic properties but retaining the interesting electronic features found in the  $\beta$ -aryl substituted compounds, we inserted in the heptakis(octylsulfanyl)- $\beta$ -aryl substituted nickel derivatives structural modifications suitable to stabilize the LC phase. Therefore we synthesized the 4-hydroxyphenyl substituted compound **12** (Scheme 2 and Chart), in which the hydroxylic substituent could stabilize intermolecular interactions by means of H-bonding, and the alkynylphenyl substituted derivative **9b** in which the triple bond acts as a “spacer” between the macrocycle and the aryl substituent allowing a better coplanarity of these two last moieties.

The mesomorphic behavior of compound **12** was investigated by crossed polarizers optical microscopy. To prevent the sample from undergoing mechanical stress it was placed between two microscope cover slides during the analysis. During the first heating of the solid sample, obtained by solution evaporation a morphological change ascribable to an LC phase, although with an undefined texture, was observed at  $T = 47.0^\circ\text{C}$ . Further heating led to melting to the liquid phase at  $T = 110.0^\circ\text{C}$ . Subsequent cooling ( $5^\circ\text{C}/\text{min}$ ) from the isotropic liquid led at  $T = 108.2^\circ\text{C}$  to the appearance of focal-conic or fan-shaped texture under crossed-polarizer (Figure 9a) and of dendritic leaflike structures without crossed polarizers. These textures strongly suggest columnar mesophases of hexagonal symmetry ( $\text{Col}_h$ ).<sup>16,35,36</sup> This LC phase evolved, at  $T = 64.7^\circ\text{C}$ , to a fingerprint texture (Figure 9b) which could be ascribable to either columnar hexagonal<sup>37</sup> or rectangular<sup>36a,c</sup> mesophases and further cooling led to crystallization of the sample at  $T = 45.4^\circ\text{C}$ . This compound showed an *enantiotropic* mesomorphism, considering that the same phase transitions reappeared during the consecutive heating and cooling processes without significant supercooling phenomena. Noteworthy, compound **12** showed a thermal range of mesophase stability of  $\Delta T = 63.0^\circ\text{C}$  which is at least  $27.0^\circ\text{C}$  wider than that observed for the previously studied  $\beta$ -phenyl substituted porphyrazine **14**.<sup>18</sup> This  $\Delta T$  widening is mainly due to the increasing of the isotropization temperature  $T_i$ . It is known that in alkyl(thio)porphyrazines the formation of LC phases is determined by the concomitant presence of different intermolecular forces, as  $\pi$ - $\pi$  interactions between the aromatic rings (for the 'free-base' porphyrazines), Van der Waals interactions of the peripheral chains, static dipole-dipole interactions (for the non-symmetric porphyrazines), and

metal-sulfur interactions between adjacent rings (for metalloporphyrines).<sup>12,16,38,39</sup> Moreover, Molecular Dynamics simulations on porphyrine metal complexes at the isotropic to LC phase transition<sup>40</sup> have shown that the process of columnar arrangement build up is driven by a starting intermolecular organization of the porphyrine central cores. Therefore the isotropization temperature can be considered a parameter strictly connected to such core-core interactions. In compound **12** the increasing of  $T_i$  in respect to the simpler phenyl substituted compound **14** reveals stronger intermolecular interactions, which could be ascribed to either the presence of stabilizing H-bonding or the increase of the dipole moment determined by the OH moiety.

The optical microscopic analysis of compound **9b** showed more interesting results. During the first heating (at 5°C/min), the solid sample transformed at  $T = 65.2^\circ\text{C}$  to a LC birefringent texture which cleared at  $T = 139.0^\circ\text{C}$ . Subsequent cooling from the isotropic melt led at  $T = 135.0^\circ\text{C}$  to the growth of the same fan shaped texture as in **12**, typical of a hexagonal columnar mesophase (Figure 10a). Upon cooling this texture transformed at  $T = 44.8^\circ\text{C}$  into a fingerprint one (Figure 10b). This texture was preserved till  $-3.0^\circ\text{C}$  when the sample crystallized. The second heating run showed, at about  $T = 61.0^\circ\text{C}$ , the transition from the solid to the fingerprint LC texture which rapidly evolved to the fan shaped one. The further cooling process exhibited the same texture modifications observed before. These data showed that **9b** displays the widest range of mesophase stability ( $\Delta T = 73.8^\circ\text{C}$  as resulted by the first heating process) in respect to that of the other non-symmetric  $\beta$ -aryl substituted compounds **12** and **14** (Chart). Therefore we decided to investigate in deeper detail its mesomorphic behaviour by DSC. The profile reported in Figure 11, obtained at a rate of 5°C/min on increasing the temperature from the crystalline to the isotropic phase, clearly showed polymorphism of the solid phase with two transitions at  $T = 53.8^\circ\text{C}$  ( $\Delta H = 6.6 \text{ Jg}^{-1}$ ) and  $64.9^\circ\text{C}$  ( $\Delta H = 19.2 \text{ Jg}^{-1}$ ) and a hardly detectable LC→liquid transition at around  $T = 140^\circ\text{C}$ . On decreasing the temperature from the liquid phase to the crystalline phase, apparently only one mesophase is detected. The thermogram showed only two exothermic peaks corresponding to the liquid→LC transition at  $136.4^\circ\text{C}$  ( $\Delta H = -0.9 \text{ Jg}^{-1}$ ) and to the LC→solid transition at  $-3.9^\circ\text{C}$  ( $\Delta H = -17.8 \text{ Jg}^{-1}$ ). The transition between the two different mesophases, readily detected by polarizing microscopy because of the sharp texture changes, was not observed by DSC. Probably this is due to the low transition enthalpy or to a second order phase transition. Variable temperature powder X-ray diffraction (PXRD) investigations

were also performed on compound **9b** in order to clarify the nature of the mesophase. The PXRD pattern recorded on cooling at 110 °C and cooling rate of 5.0°C/min showed the presence of four small angle reflections with reciprocal spacings in the ratio  $1:\sqrt{3}:\sqrt{4}:\sqrt{7}$ , corresponding to the indexation (10), (11), (20) and (21), characteristic of a two-dimensional hexagonal lattice ( $\text{Col}_h$ ) (Figure S4 in ESI) with the cell parameter  $a$  of 23.9 Å. Additionally, in the wide angle region, a diffuse halo at  $\approx 4.4$  Å is present corresponding to the liquid like disorder of the aliphatic chains. The same PXRD pattern was recorded at room temperature, where a fingerprint texture was observed. This observation proved that the liquid crystalline state was maintained up to room temperature and that the two mesophases detected have different texture but the same hexagonal packing. Similar findings have been reported in the literature where it has been shown that in compounds displaying multiple  $\text{Col}_h$  phases, cooling to lower temperature the  $\text{Col}_h$  phase can transform the fan textures into fingerprint textures.<sup>37,41</sup> If left on standing at room temperature for a week the LC sample froze, as shown both by PXRD analysis and optical microscopy. Therefore, a supercooling phenomenon of the LC phase can be envisaged and the columnar arrangement, retained up to room temperature, is metastable.

In summary, as far as the heptakis(octylsulfanyl)- $\beta$ -phenyl porphyrazine derivatives are concerned, we observed that the ‘free base’ compound **13** does not show any LC behaviour, while its Ni(II) complex **14** presents a columnar hexagonal mesophase with stability range of  $\Delta T = 36.0^\circ\text{C}$ .<sup>18</sup> The insertion of an ethynyl “spacer” in between the macrocycle and the phenyl moiety in **9b** gives rise to a doubling of the thermal stability range of the mesophase which reach  $\Delta T = 73.8^\circ\text{C}$ . Taking into account that, as shown above, the presence of the triple bond does not interfere on the electron transfer between the aryl moiety and the macrocycle, but strongly improve the mesomorphic properties of these aryl-substituted porphyrazines, we can envisage that arylacetylenic derivatives could be compounds suitable for optoelectronic and endowed with self-aggregation properties.

## Conclusions

We described herein the synthesis of a series of novel non-symmetrically substituted mono  $\beta$ -aryl and  $\beta$ -arylethynyl (alkylsulfanyl)porphyrazines as well as their Ni(II) complexes and a detailed experimental and computational study of their spectral, electrochemical, and

mesomorphic properties. These substrates were prepared by Suzuki-Miyaura and Sonogashira cross-coupling reactions, applying for the first time these Pd(0) catalysed cross-coupling procedures on porphyrazine tetrapyrroles. Electrochemistry studies showed that in the prepared compounds the macrocyclic ring is the main responsible of the reduction process and is perturbed by the aryl substituent. The highest perturbation of the porphyrazine  $\pi$ -electron core is provided by strong electron-donating (NMe<sub>2</sub>) and electron withdrawing (NO<sub>2</sub>) aryl substituents, which increase and decrease the macrocycle electron density, respectively. A strong influence of the amino and nitro substituents was also noticed on the UV-Vis spectra, where absorptions having a charge-transfer character were present as a 800 nm Q band tail and as a low-energy Soret shoulder, respectively. Computational TDDFT studies showed that while in most of the compounds the LUMOs and HOMOs are mainly localized on the porphyrazine ring, in the amino-substituted derivatives **7**, **8**, and **11** the LUMO is localized on the peripheral aryl moieties and the HOMO on the macrocycle. In these compounds the HOMO-LUMO electronic transition give rise to the above mentioned charge-transfer absorptions. On the contrary, in the nitro compound **10** the charge transfer absorption is due to transitions going backward from macrocycle-localized HOMOs orbitals to aryl-localized LUMO+2 orbital. Therefore, in these mono aryl-substituted porphyrazines the macrocyclic ring has an ambivalent behavior, acting as an electron acceptor in the case of the NMe<sub>2</sub> substituted compounds and as an electron donor in the NO<sub>2</sub> substituted derivative. They thus provide unconventional “push-pull” or, as recently defined,<sup>7</sup> “push-no-pull” systems suitable for NLO. Notably, all the studied compounds display HOMO levels lower than -5.2 eV and HOMO-LUMO bandgaps in the 1.3-1.8 range which make these aryl- and arylethynyl-substituted porphyrazines also possible candidates for PCBM-based organic photovoltaic devices. Finally, columnar discotic mesophases have been also shown by thio-octyl arylethynyl derivatives, allowing to envisage the possibility to achieve compounds both suitable for optoelectronic and endowed with self-aggregation properties.

## Experimental

### *Synthesis*

All chemicals and solvents (Aldrich Chemicals Ltd.) were of reagent grade. Solvents were dried and distilled before use according to standard procedures. Solvents used in physical measurements were of spectroscopic or HPLC grade. Silica gel used for chromatography was Merck Kieselgel 60 (70-230 mesh). For preparative TLC Merck 0.5 mm F<sub>254</sub> silica on glass plates was used. <sup>1</sup>H NMR spectra were recorded on a 500 or 400 MHz INOVA Varian spectrometer with SiMe<sub>4</sub> as internal standard. Mass spectra were acquired in positive reflectron mode at 20 kV using Ettan MALDI-TOF Pro mass spectrometer (Amersham Biosciences) equipped with an UV nitrogen laser (337 nm) with delayed extraction mode and low mass rejection. For each spectrum 256 single shots were accumulated. Spectra were externally calibrated using two standard peptides (ile- Ang III, M+H 897.531 and hACTH 18-39, M+H 2465.199, monoisotopics). The matrix was prepared mixing 1% (w/v) alpha-cyano-4-hydroxy-cinnamic acid solution, 50% acetonitrile (v/v), and 0.5% (v/v) trifluoroacetic acid. Samples for mass spectrometric analysis were prepared by dissolving 4 μL of porphyrazine solution (<10<sup>-4</sup> M in CH<sub>2</sub>Cl<sub>2</sub>) directly in 4 μL of the matrix. 0.4 μL of this mixture was deposited on the probe tip and allowed to evaporate.

The non-symmetrically H-substituted 'free-base' porphyrazines **2a**<sup>11</sup> and **2b**,<sup>12</sup> the Br-substituted 'free-base' porphyrazine **3b**<sup>12</sup> and the corresponding nickel (II) complex **4b**<sup>18</sup> were prepared according to previously described procedures.

#### **2-Bromo-3,7,8,12,13,17,18-Heptakis(ethylsulfanyl)-5,10,15,20-21H,23H-porphyrazine**

**(3a)**. The compound was synthesised using a reported procedure.<sup>12,18</sup> Pure **3a** was obtained in 90% yield after column chromatography of the crude on silica gel using CH<sub>2</sub>Cl<sub>2</sub>-*n*-hexane (1:1, v/v) as eluent (first band, R<sub>f</sub> 0.44). <sup>1</sup>H NMR (400 MHz, CDCl<sub>3</sub>, 297 K), δ/ppm: 4.45 (q, *J* = 7.5 Hz, 2H, SCH<sub>2</sub>), 4.22-4.00 (m, 12H, SCH<sub>2</sub>), 1.67 (t, *J* = 7.5 Hz, 3H, CH<sub>3</sub>), 1.62-1.52 (m, 18H, CH<sub>3</sub>), -1.60 (s, 2H, NH). MALDI-MS: *m/z* 812.88 [M+H]<sup>+</sup> (calc. 813.04).

#### **[2-Bromo-3,7,8,12,13,17,18-Heptakis(ethylsulfanyl)-5,10,15,20-porphyrinato] nickel**

**(II) (4a)**. The complex **4a** was prepared starting from compound **3a** according to the previously reported procedure for the synthesis of similar nickel(II) (alkylsulfanyl)porphyrazines.<sup>16b</sup> Pure **4a** was obtained in 72% yield after column chromatography of the crude on silica gel using CH<sub>2</sub>Cl<sub>2</sub>-*n*-hexane (1:1, v/v) as eluent (second band, R<sub>f</sub> 0.36), followed by preparative TLC on silica gel plate with the same eluent mixture. <sup>1</sup>H NMR (500 MHz, CDCl<sub>3</sub>, 297 K), δ/ppm : 4.27 (q, *J* = 7.5 Hz, 2H, SCH<sub>2</sub>), 4.12-4.02 (m,

8H, SCH<sub>2</sub>), 3.99 (q,  $J = 7.5$  Hz, 2H, SCH<sub>2</sub>), 3.94 (q,  $J = 7.5$  Hz, 2H, SCH<sub>2</sub>), 1.7-1.47 (m, 21H, CH<sub>3</sub>). MALDI-MS:  $m/z$  869.03 [M+H]<sup>+</sup> (calc. 868.96).

**Suzuki cross-coupling reaction. General procedure.**

Non-symmetric brominated porphyrazine **3** (0.07 mmol), potassium carbonate (0.56 mmol), tetrakis(triphenylphosphine)-palladium(0) (10% mol) and the corresponding boronic acid (0.28 mmol) were refluxed in a dry DMF/toluene (2:3, v/v) mixture (10 mL) under N<sub>2</sub>. The reaction was monitored by TLC and stopped after 12–18 h, depending on the substrate. After cooling to room temperature water was added and the solution was extracted with CH<sub>2</sub>Cl<sub>2</sub>. The organic fractions were collected, dried over sodium sulphate and filtered. After removal of the solvent under reduced pressure, the crude product was purified by column chromatography on silica gel using a CH<sub>2</sub>Cl<sub>2</sub>–*n*-hexane mixture as eluent.

**2-(4-Trifluoromethylphenyl)-3,7,8,12,13,17,18-Heptakis(ethylsulfanyl)-5,10,15,20–21H,23H-porphyrazine (5).** Compound **5** was obtained by Suzuki cross-coupling of **3a** and 4-trifluoromethylphenyl boronic acid. Pure compound was isolated in 20% yield after purification by column chromatography on silica gel with a CH<sub>2</sub>Cl<sub>2</sub>–*n*-hexane (1:1) mixture as eluent (second band, R<sub>f</sub> 0.56). <sup>1</sup>H NMR (500 MHz, CDCl<sub>3</sub>, 297 K),  $\delta$ /ppm: 8.53 (d,  $J = 8.0$  Hz, 2H, ArH), 8.03 (d,  $J = 8.0$  Hz, 2H, ArH), 4.25-4.10 (m, 6H, SCH<sub>2</sub>), 4.08 (q,  $J = 7.5$  Hz, 2H, SCH<sub>2</sub>), 4.03 (q,  $J = 7.5$  Hz, 2H, SCH<sub>2</sub>), 4.00 (q,  $J = 7.5$  Hz, 2H, SCH<sub>2</sub>), 3.89 (q,  $J = 7.5$  Hz, 2H, SCH<sub>2</sub>), 1.65-1.55 (m, 12H, CH<sub>3</sub>), 1.53 (t,  $J = 7.5$  Hz, 3H, CH<sub>3</sub>), 1.46 (t,  $J = 7.5$  Hz, 3H, CH<sub>3</sub>), 1.39 (t,  $J = 7.5$  Hz, 3H, CH<sub>3</sub>), -1.41 (s, 2H, NH). MALDI-MS:  $m/z$  878.98 [M+H]<sup>+</sup> (calc. 879.15).

**2-(4-Trifluoromethoxyphenyl)-3,7,8,12,13,17,18-Heptakis(ethylsulfanyl)-5,10,15,20–21H,23H-porphyrazine (6).** Compound **6** was obtained by Suzuki cross-coupling of **3a** and 4-trifluoromethoxyphenyl boronic acid. Pure compound was isolated in 23% yield after purification by column chromatography on silica gel with a CH<sub>2</sub>Cl<sub>2</sub>–*n*-hexane (1:1) mixture as eluent (second band, R<sub>f</sub> 0.55). <sup>1</sup>H NMR (500 MHz, CDCl<sub>3</sub>, 297 K),  $\delta$ /ppm: 8.47 (d,  $J = 8.5$  Hz, 2H, ArH), 8.63 (d,  $J = 8.5$  Hz, 2H, ArH), 4.20-4.10 (m, 6H, SCH<sub>2</sub>), 4.09 (q,  $J = 7.5$  Hz, 2H, SCH<sub>2</sub>), 4.04 (q,  $J = 7.5$  Hz, 2H, SCH<sub>2</sub>), 4.03 (q,  $J = 7.5$  Hz, 2H, SCH<sub>2</sub>), 3.93 (q,  $J = 7.5$  Hz, 2H, SCH<sub>2</sub>), 1.62-1.55 (m, 12H, CH<sub>3</sub>), 1.53 (t,  $J = 7.5$  Hz, 3H, CH<sub>3</sub>), 1.47 (t,  $J = 7.5$  Hz,

3H, CH<sub>3</sub>), 1.41 (t,  $J = 7.5$  Hz, 3H, CH<sub>3</sub>), -1.21 (s, 2H, NH). MALDI-MS:  $m/z$  894.98 [M+H]<sup>+</sup> (calc. 895.15).

**2-(4-*N,N*-Dimethylaminophenyl)-3,7,8,12,13,17,18-Heptakis(ethylsulfanyl)-5,10,15,20-21*H*,23*H*-porphyrazine (7).** Compound **7** was obtained by Suzuki cross-coupling of **3a** and 4-*N,N*-Dimethylaminophenyl boronic acid. Pure **7** was isolated in 15% yield after purification by column chromatography on silica gel with a CH<sub>2</sub>Cl<sub>2</sub>-*n*-hexane (7:3) mixture as eluent (second band,  $R_f$  0.61), followed by preparative TLC on silica gel plate with the same eluent mixture. <sup>1</sup>H NMR (500 MHz, CDCl<sub>3</sub>, 297 K),  $\delta$ /ppm: 8.57 (d,  $J = 8.5$  Hz, 2H, ArH), 7.12 (d,  $J = 8.5$  Hz, 2H, ArH), 4.18 (q,  $J = 7.5$  Hz, 2H, SCH<sub>2</sub>), 4.16 (q,  $J = 7.5$  Hz, 2H, SCH<sub>2</sub>), 4.10 (q,  $J = 7.5$  Hz, 2H, SCH<sub>2</sub>), 4.08 (q,  $J = 7.5$  Hz, 2H, SCH<sub>2</sub>), 4.02 (q,  $J = 7.5$  Hz, 2H, SCH<sub>2</sub>), 4.00 (q,  $J = 7.5$  Hz, 2H, SCH<sub>2</sub>), 3.99 (q,  $J = 7.5$  Hz, 2H, SCH<sub>2</sub>), 1.62-1.53 (m, 12H, CH<sub>3</sub>), 1.53 (t,  $J = 7.5$  Hz, 3H, CH<sub>3</sub>), 1.45 (t,  $J = 7.5$  Hz, 3H, CH<sub>3</sub>), 1.43 (t,  $J = 7.5$  Hz, 3H, CH<sub>3</sub>), -1.10 (s, 2H, NH). MALDI-MS:  $m/z$  855.03 [M+2H]<sup>+</sup> (calc. 855.23).

**[2-(4-*N,N*-dimethylaminophenyl)-3,7,8,12,13,17,18-Heptakis(ethylsulfanyl)-5,10,15,20-porphyrazinato] nickel (II) (8).** The complex **8** was prepared starting from compound **7** according to the previously reported procedure for the synthesis of similar nickel(II) (alkylsulfanyl)porphyrazines.<sup>16b</sup> Pure **8** was obtained in 40% yield after column chromatography of the crude on silica gel using CH<sub>2</sub>Cl<sub>2</sub>-*n*-hexane (1:1, v/v) as eluent (second band,  $R_f$  0.25), followed by preparative TLC on silica gel plate with the same eluent mixture. <sup>1</sup>H NMR (500 MHz, CDCl<sub>3</sub>, 297 K),  $\delta$ /ppm : 8.38 (d,  $J = 8.5$  Hz, 2H, ArH), 7.02 (d,  $J = 8.5$  Hz, 2H, ArH), 4.05-3.90 (m, 10H, SCH<sub>2</sub>), 3.81 (q,  $J = 7.5$  Hz, 2H, SCH<sub>2</sub>), 3.77 (q,  $J = 7.5$  Hz, 2H, SCH<sub>2</sub>), 1.50-1.40 (m, 15H, CH<sub>3</sub>), 1.33 (t,  $J = 7.5$  Hz, 3H, CH<sub>3</sub>), 1.31 (t,  $J = 7.5$  Hz, 3H, CH<sub>3</sub>). MALDI-MS:  $m/z$  909.99 [M+H]<sup>+</sup> (calc. 910.13).

**[2-(4-Hydroxyphenyl)-3,7,8,12,13,17,18-Heptakis(octylsulfanyl)-5,10,15,20-porphyrazinato] nickel (II) (12).** Compound **12** was obtained by Suzuki cross-coupling of **3b** and 4-hydroxyphenyl boronic acid. Pure **12** was isolated in 22% yield after purification by column chromatography on silica gel with a CH<sub>2</sub>Cl<sub>2</sub>-*n*-hexane (3:7) mixture as eluent (second band,  $R_f$  0.42), followed by preparative TLC on silica gel plate with the same eluent mixture. <sup>1</sup>H NMR (400 MHz, CDCl<sub>3</sub>, 297 K),  $\delta$ /ppm: 7.34 (dd,  $J' = J'' = 8.0$  Hz, 2H, ArH), 7.25 (dd,  $J' = J'' = 8.0$  Hz, 2H, ArH), 7.11 (t,  $J = 7.5$  Hz, 1H, OH), 4.14 (t,  $J = 7.5$  Hz, 2H, SCH<sub>2</sub>), 4.10-

3.90 (m, 8H, SCH<sub>2</sub>), 3.62 (t,  $J = 7.5$  Hz, 2H, SCH<sub>2</sub>), 3.43 (t,  $J = 7.5$  Hz, 2H, SCH<sub>2</sub>), 1.76-1.96 (m, 14H, CH<sub>2</sub>), 1.40-1.66 (m, 14H, CH<sub>2</sub>), 1.40-1.10 (m, 56H, CH<sub>2</sub>), 0.70-0.90 (m, 21H, CH<sub>3</sub>). MALDI-MS:  $m/z$  1471.92 [M+H]<sup>+</sup> (calc. 1471.74); 1494.97 [M+H+Na]<sup>+</sup> (calc. 1494.73).

#### Sonogashira cross-coupling reaction. General procedure.

A mixture of the brominated Ni(II)porphyrazine **4a** or **4b** (100.0 mg, 69.0  $\mu$ mol), dichlorobis-(triphenylphosphine)-palladium(II) Pd(PPh<sub>3</sub>)<sub>2</sub>Cl<sub>2</sub> (3.8 mg, 5.5  $\mu$ mol), CuI (2.6 mg, 13.8  $\mu$ mol), arylalkyne (8.5 mg, 82.8  $\mu$ mol) and anhydrous triethylamine (1.0 mL) in THF (5.5 mL) was stirred at room temperature under an argon atmosphere for 2h. After removal of the volatiles in vacuo, the dark solid residue was extracted with CH<sub>2</sub>Cl<sub>2</sub>. The organic phase was washed with water, then collected, dried over anhydrous sodium sulphate and filtered. After removal of the solvent under reduced pressure, the crude product was purified by column chromatography on silica gel using a CH<sub>2</sub>Cl<sub>2</sub>-*n*-hexane mixture as eluent.

#### [2-(Ethynylphenyl)-3,7,8,12,13,17,18-Heptakis(ethylsulfanyl)-5,10,15,20-

**porphyrazinato] nickel (II) (9a).** Compound **9a** was obtained by Sonogashira cross-coupling of **4a** and phenylacetylene. Pure compound was isolated in 30% yield after purification by column chromatography on silica gel with a CH<sub>2</sub>Cl<sub>2</sub>-*n*-hexane (1:1) mixture as eluent (second band,  $R_f$  0.25), followed by preparative TLC on silica gel plate with the same eluent mixture. <sup>1</sup>H NMR (500 MHz, CDCl<sub>3</sub>, 297 K),  $\delta$ /ppm: 7.82-7.74 (m, 2H, ArH), 7.52-7.40 (m, 3H, ArH), 4.22 (q,  $J = 7.5$  Hz, 2H, SCH<sub>2</sub>), 4.02 (q,  $J = 7.5$  Hz, 4H, SCH<sub>2</sub>), 3.99 (q,  $J = 7.5$  Hz, 2H, SCH<sub>2</sub>), 3.98 (q,  $J = 7.5$  Hz, 2H, SCH<sub>2</sub>), 3.90 (q,  $J = 7.5$  Hz, 2H, SCH<sub>2</sub>), 3.88 (q,  $J = 7.5$  Hz, 2H, SCH<sub>2</sub>), 1.68 (t,  $J = 7.5$  Hz, 3H, CH<sub>3</sub>), 1.62-1.38 (m, 18H, CH<sub>3</sub>). MALDI-MS:  $m/z$  890.87 [M+H]<sup>+</sup> (calc. 891.085); 908.87 [M+H<sub>2</sub>O+H]<sup>+</sup> (calc. 909.09); 931.05 [M+H<sub>2</sub>O+Na]<sup>+</sup> (calc. 931.08).

#### [2-(Ethynylphenyl)-3,7,8,12,13,17,18-Heptakis(octylsulfanyl)-5,10,15,20-

**porphyrazinato] nickel (II) (9b).** Compound **9b** was obtained by Sonogashira cross-coupling of **4b** and phenylacetylene. Pure compound was isolated in 28% yield after purification by column chromatography on silica gel with a CH<sub>2</sub>Cl<sub>2</sub>-*n*-hexane (3:7) mixture as eluent (second band,  $R_f$  0.37), followed by preparative TLC on silica gel plate with the same eluent mixture. <sup>1</sup>H NMR (500 MHz, CDCl<sub>3</sub>, 297 K),  $\delta$ /ppm: 7.86 (d,  $J = 7.5$  Hz, 2H,

ArH), 7.52 (dd,  $J' = J'' = 7.5$  Hz, 2H, ArH), 7.48 (t,  $J = 7.5$  Hz, 1H, ArH), 4.22 (t,  $J = 7.5$  Hz, 2H, SCH<sub>2</sub>), 4.14-3.98 (m, 8H, SCH<sub>2</sub>), 3.98-3.90 (m, 4H, SCH<sub>2</sub>), 2.12-2.00 (m, 2H, CH<sub>2</sub>), 1.90-1.70 (m, 12H, CH<sub>2</sub>), 1.70-1.50 (m, 14H, CH<sub>2</sub>), 1.50-1.00 (m, 56H, CH<sub>2</sub>), 0.90-0.70 (m, 21H, CH<sub>3</sub>). MALDI-MS:  $m/z$  1479.72 [M+H]<sup>+</sup> (calc. 1479.72).

**[2-(Ethynyl-4-nitrophenyl)-3,7,8,12,13,17,18-Heptakis(ethylsulfanyl)-5,10,15,20-porphyrazinato] nickel (II) (10).** Compound **10** was obtained by Sonogashira cross-coupling of **4a** and 4-nitrophenylacetylene. Differently to the general procedure, the reaction mixture was heated at reflux, under an argon atmosphere for 5h. Pure compound was isolated in 33% yield after purification by column chromatography on silica gel with a CHCl<sub>3</sub>-*n*-hexane (8:2) mixture as eluent (second band, R<sub>f</sub> 0.87), followed by preparative TLC on silica gel plate with the same eluent mixture. <sup>1</sup>H NMR (500 MHz, CDCl<sub>3</sub>, 297 K),  $\delta$ /ppm: 8.42 (dd,  $J' = J'' = 7.5$  Hz, 2H, ArH), 7.99 (dd,  $J' = J'' = 7.5$  Hz, 2H, ArH), 4.20-4.35 (m, 2H, SCH<sub>2</sub>), 4.20-3.90 (m, 12H, SCH<sub>2</sub>), 1.80-1.70 (m, 3H, CH<sub>2</sub>), 1.68-1.40 (m, 18H, CH<sub>3</sub>). MALDI-MS:  $m/z$  935.79 [M+H]<sup>+</sup> (calc. 936.07), 953.81 [M+H<sub>2</sub>O+H]<sup>+</sup> (calc. 954.08).

**[2-(Ethynyl-4-*N,N*-dimethylaminophenyl)-3,7,8,12,13,17,18-Heptakis(ethylsulfanyl)-5,10,15,20-porphyrazinato] nickel (II) (11).** Compound **11** was obtained by Sonogashira cross-coupling of **4a** and 4-*N,N*-dimethylaminophenylacetylene. Pure compound was isolated in 27% yield after purification by column chromatography on silica gel with a CH<sub>2</sub>Cl<sub>2</sub>-*n*-hexane (1:1) mixture as eluent (third band, R<sub>f</sub> 0.11), followed by preparative TLC on silica gel plate with the same eluent mixture. <sup>1</sup>H NMR (500 MHz, CDCl<sub>3</sub>, 297 K),  $\delta$ /ppm: 7.67 (d,  $J = 8.5$  Hz, 2H, ArH), 6.80 (d,  $J = 8.5$  Hz, 2H, ArH), 4.35-4.15 (m, 4H, SCH<sub>2</sub>), 4.15-3.85 (m, 10H, SCH<sub>2</sub>), 1.71 (t,  $J = 7.5$  Hz, 3H, CH<sub>3</sub>), 1.60-1.45 (m, 18H, CH<sub>3</sub>). MALDI-MS:  $m/z$  934.13 [M+H]<sup>+</sup> (calc. 934.13), 952.08 [M+H<sub>2</sub>O+H]<sup>+</sup> (calc. 952.14).

### Instrumental characterization

Solution electronic spectra in 1 cm path length quartz cells in the region 300-800 nm were performed on a UV-Vis-NIR 05E Cary spectrophotometer (the concentration of the solutions was *ca.* 10<sup>-6</sup>M in compound).

The cyclic voltammetry (CV) and differential pulse voltammetry (DPV) experiments were performed with an EG & G Princeton Applied Research Model 263A Potentiostat/Galvanostat. Data were collected and analyzed by the Model 270 electrochemical analysis system software

on a PC computer.<sup>42</sup> A standard three-electrode arrangement was employed. The working electrode was a glassy carbon button ( $\varnothing = 3$  mm). A platinum wire served as counter electrode and a home-made AgCl/Ag electrode containing saturated KCl was used as the reference electrode. All the oxidation and reduction potentials are reported relative to the ferrocene/ferrocenium ( $\text{Fc}/\text{Fc}^+$ ) potential scale, using the voltammetric oxidation of ferrocene as an internal reference. The reproducibility of individual potential values was within  $\pm 5$  mV. All the electrochemical measurements were carried out using Schlenk techniques (Argon) at room temperature in  $\text{CH}_2\text{Cl}_2$  and solvent (from Aldrich) were dried and distilled before use by standard methods. The concentration of the supporting electrolyte  $[\text{N}(\text{C}_4\text{H}_9)_4\text{BF}_4]$  was typically of 0.15 M. Cyclic voltammograms were recorded by scanning the potential at 200  $\text{mVs}^{-1}$ . DPV measurements were performed at 5  $\text{mVs}^{-1}$  with a pulse height of 50 mV and 50 ms pulse width.

Optical observations of textures as a function of the temperature (at scanning rates of 5.0°C  $\text{min}^{-1}$ ) were performed with a Axioplan-Zeiss polarizing microscope equipped with a Linkam microfurnace. Images were captured using a Zeiss MC80 Microscope Camera and samples were studied between two silica glass plates (diameter 16.0 mm).

Transition temperatures and enthalpies were measured with a Perkin-Elmer Pyris 1 DSC instrument operated at scanning rates of 5.0°C  $\text{min}^{-1}$ . The apparatus was calibrated with indium. The sample pans and covers were made of aluminium (diameter 5.0 mm). The uncertainty in each measured temperature was  $\pm 0.1$ °C.

Powder X-ray diffraction pattern was obtained by using a Bruker AXS General Area Detector Diffraction System (D8 Discover with GADDS) with  $\text{Cu-K}\alpha$  radiation; the area detector was placed at a distance of 20 cm from the sample and at a angle  $2\theta_D$  of 12°. Measurements were performed by charging samples in Lindemann capillary tubes with inner diameters of 0.5 mm. The local temperature on the sample was changed by using a CalCTec (Italy) heating stage. The sample was heated and cooled at a rate of 5.0 °C  $\text{min}^{-1}$  to the appropriate temperature.

### Computational Methods

The Gaussian 09, Revision C.01 software<sup>43</sup> was used for all the computations. The Density Functional Theory (DFT) was applied by using the B3LYP hybrid xc functional<sup>44</sup> for geometry optimizations with the 6-31G\* basis set as implemented in the program.<sup>45</sup> Default gradient and displacement thresholds were used for the geometry optimization convergence

criteria. All the reported geometries are relative minima of the potential energy surface (electronic energy in the Born-Oppenheimer approximation), as confirmed by the analytical computation of the Hessian matrix at the same level of approximation.

The Time Dependent Density Functional Theory (TDDFT)<sup>46</sup> was applied for computing the excitation wavelengths, oscillator strengths and associated excited state composition in terms of mono-electronic excitations between occupied and unoccupied Kohn-Sham orbitals. The Gaussian 09 default approach was used for these computations.<sup>47</sup> TDDFT computations were performed with the M06 xc functional<sup>48</sup> on the B3LYP/6-31G\* structure with inclusion of solvation effects by the means of SCRf (Self Consistent Reaction Field) IEFPCM (Integral Equation Formalism Polarizable Continuum Model) as implemented in the program.<sup>49</sup>

The computed HOMO and LUMO energies in Table 1 and Figure 2 are energy differences between neutral and charged molecules ( $\Delta$ SCF). Both neutral and charged structures were optimized in vacuum at the B3LYP/6-31G\* level and, on them, single-point (SCF) IEFPCM computations were performed at the B3LYP/6-31+G\* level of approximation.

The Kohn-Sham orbitals were drawn using the program MolDen 4.9.<sup>50</sup> Orbital shapes and energies in Figures 3 and 8, were computed at the M06/6-31G\* level of approximation with inclusion of IEFPCM effects in CH<sub>2</sub>Cl<sub>2</sub> on the B3LYP/6-31G\* structure in vacuum (neutral molecules).

The same procedure was applied for the TDDFT results reported in Figures 5 and 7 and in general in the text. TDDFT results in toluene were obtained with the same procedure, these results are mentioned in the text without a graphical representation.

## References and Notes

---

- (a) G. de la Torre, P. Vazquez, F. Agulló-Lopez and T. Torres, *Chem. Rev.*, 2004, **104**, 3723-3750; (b) M. Drobizhev, N. S. Makarov, A. Rebane, G. de la Torre and T. Torres, *J. Phys. Chem. C*, 2008, **112**, 848-859; (c) M. O. Senge, M. Fazekas, E. G. A. Notaras, W. J. Blau, M. Zawadzka, O. B. Locos and E. M. N. Mhuirheartaigh, *Adv. Mater.*, 2007, **19**, 2737-2774; (d) K. McEwan, K. Lewis, G.-Y. Yang, L. -L. Chng, Y.-W. Lee, W. -P. Lau and K. -S. Lai, *Adv. Funct. Mater.*, 2003, **13**, 863-867.
- (a) R. W. Boyd, *Nonlinear Optics*, Academic Press, San Diego, CA, 1992; (b) J. Zyss, *Molecular Nonlinear Optics: Materials, Physics and Devices*, Academic Press: New York, 1994; (c) B. E. A Saleh and M. C Teich, *Fundamentals of Photonics*, Wiley, New York, 1991; (d) G. H. Wagnière, *Linear and Nonlinear Optical Properties of Molecules*, Verlag Helvetica Chimica Acta, Basel, 1993; (e) S. R. Marder, *Chem. Comm.*, 2006, 131-134; (f) P. A. Sullivan and L.R. Dalton, *Acc. Chem. Res.*, 2010, **43**, 10-18.
- (a) S. M. LeCours, H.-W. Guan, S. G. Di Magno, C. H. Wang and M. J. Thierien, *J. Am. Chem. Soc.*, 1996, **118**, 1497-1503; (b) S. Priyadarshy, M. J. Thierien and D. N. Beratan, *J. Am. Chem. Soc.*, 1996, **118**, 1504-1510; (c) L. Karki, F. W. Vance, J. T. Hupp, S. M. LeCours and M. J. Thierien, *J. Am. Chem. Soc.*, 1998, **120**, 2606-2611; (d) M. Yeung, A. C. H. Ng, M. G. B. Drew, E. Vorpapel, E. M. Breitung, R. J. McMahon and D. K. P. Ng, *J. Org. Chem.*, 1998, **63**, 7143-7150; (e) T.-G. Zhang, Y. Zhao, I. Asselberghs, A. Peersons, K. Clays, and M. J. Thieren, *J. Am. Chem. Soc.*, 2005, **127**, 9710-9720; (f) T.-G. Zhang, Y. Zhao, K. Song, I. Asselberghs, A. Peersons, K. Clays and M. J. Thieren, *Inorg. Chem.*, 2006, **45**, 9703-9712; (g) T. Ishizuka, L.E. Sinks, K. Song, S.-T. Hung, A. Nayak, K. Clays and M. J. Thieren, *J. Am. Chem. Soc.*, 2011, **133**, 2884-2896; (h) N. Jiang, G. Zuber, S. Keinan, A. Nayak, W. Yang, M. J. Thieren and D. N. Beratan, *J. Phys. Chem. C.*, 2012, **116**, 9724-9733.
- (a) K. S. Suslick, C. T. Chen, G. R. Meredith and L.-T. Cheng, *J. Am. Chem. Soc.*, 1992, **114**, 6928-6930; (b) M. Yeung, A. C. H. Ng, M. G. B. Drew, E. Vorpapel, E. M. Breitung, R. J. McMahon and D. K. P. Ng, *J. Org. Chem.*, 1998, **63**, 7143-7150; (c) I. D. L. Albert, T. J. Marks and M. A. Ratner, *Chem. Mater.* 1998, **10**, 753-762; (d) E.

- 
- Annoni, M. Pizzotti, R. Ugo, S. Quici, T. Morotti, M. Bruschi and P. Mussini, *Eur. J. Inorg. Chem.* 2005, 3857-3874.
5. (a) A. Sastre, B. del Rey and T. Torres, *J. Org. Chem.*, 1996, **61**, 8591-8597; (b) A. Sastre, M. A. Díaz-García, B. del Rey, C. Dhenaut, J. Zyss, I. Ledoux, F. Agulló-López and T. Torres, *J. Phys. Chem. A*, 1997, **101**, 9773-9777; (c) E. M. Maya, E. M. García-Frutos, P. Vazquez, T. Torres, G. Martín, G. Rojo, F. Agulló-López, R. H. Gonzalez-Jonte, V. R. Ferro, J. M. García de la Vega, I. Ledoux and J. Zyss, *J. Phys. Chem. A*, 2003, **107**, 2110-2117; (d) N. Kobayashi, N. Sasaki, Y. Higashi and T. Osa, *Inorg. Chem.* 1995, **34**, 1636-1637; (e) N. Kobayashi, Y. Kobayashi and T. Osa, *J. Am. Chem. Soc.*, 1993, **115**, 10994-10995.
6. M. G. Walter, A. B. Rudine and C. C. Wamser, *J. Porphyrins Phthalocyanines*, 2010, **14**, 759-792 and references therein.
7. I. Lopez-Duarte, J. E. Reeve, J. Pérez-Moreno, I. Boczarow, G. Depotter, J. Fleischhauer, K. Clays and H. L. Anderson, *Chem. Sci.*, 2013, **4**, 2024-2027.
8. (a) C. C. Leznoff and A. B. P. Lever, In *Phthalocyanines, Properties and Applications Vols 1-4*; VCH, New York, 1989-1996; (b) P. A. Stuzhin, C. Ercolani, in *The Porphyrin Handbook*, ed. K. M. Kadish, K. M. Smith, R. Guilard, Academic Press, New York, 2003, vol 15, p. 263; (c) D. Dolphin, In *The Porphyrins, Vols 1-7*; Academic: New York, 1978-1979; (d) T. P. Forsyth, D. B. G. Williams, A. G. Montalban, C. L. Stern, A. G. M. Barrett and B. M. Hoffman, *J. Org. Chem.*, 1998, **63**, 331-336.
9. (a) H. S. Nalwa, M. Hanack, G. Pawlowski and M. K. Engel, *Chem. Phys.*, 1999, **245**, 17-26; (b) T. C. Wen and C. J. Tsai, *Chem. Phys. Lett.*, 1999, **311**, 173-178; (c) M. P. Donzello, Z. Ou, D. Dini, M. Meneghetti, C. Ercolani, and K. M. Kadish, *Inorg. Chem.*, 2004, **43**, 8637-8648; (d) M. P. Donzello, C. Ercolani and P. A. Stuzhin, *Coord. Chem. Rev.*, 2006, **250**, 1530-1561; (e) S. Vagin, M. Barthel, D. Dini and M. Hanack, *Inorg. Chem.*, 2003, **42**, 2683-2694; (f) M. Hanack, D. Dini, M. Barthel and S. Vagin, *Chem. Record*, 2002, **2**, 129-148; (g) M. P. Donzello, D. Dini, G. D'Arcangelo, C. Ercolani, R. Zhan, Z. Ou, P. A. Stuzhin and K. M. Kadish., *J. Am. Chem. Soc.*, 2003, **125**, 14190-14204.

- 
10. For NLO studies of non symmetric porphyrazines see: (a) S. Vagin, G. Y. Yang, M. K. Y. Lee, M. Hanack, *Opt. Commun.*, 2003, **228**, 119-125; (b) S. Vagin, M. Hanack, *Eur. J. Org. Chem.*, **2002**, 2859-2865.
  11. S. Belviso, G. Ricciardi, F. Lelj, L. Monsù Scolaro, A. Bencini and C. Carbonera, *J. Chem. Soc., Dalton Trans.*, 2001, 1143-1150.
  12. S. Belviso, A. Giugliano, M. Amati, G. Ricciardi, F. Lelj and L. Monsù Scolaro, *Dalton Trans.*, 2004, 305-312.
  13. I. C. Khoo, *Physics Reports*, 2009, **471**, 221-267.
  14. For some examples concerning NLO properties of discotic LC see: (a) L. R. Milgrom, G. Yahioğlu, D. W. Bruce, S. Morrone, F. Z. Henari and W. J. Blau, *Adv. Mater.*, 1997, **9**, 313-316; (b) S. H. Kang, Y. -S. Kang, W. -C. Zin, G. Olbrechts, K. Wostyn, K. Clays, A. Persoons and K. Kim, *Chem. Commun.*, 1999, 1661-1662; (c) H. Lee, D. Kim, H. -K. Lee, W. Qiu, N. -K. Oh, W. -C. Zin and K. Kim, *Tetrahedron Lett.*, 2004, **45**, 1019-1022.
  15. (a) J. Nelson, *Science*, 2001; **293**: 1059-1060; (b) L. Schmidt-Mende, A. Fechtenkotter, K. Mullen, E. Moons, R. H. Friend and J. D. MacKenzie, *Science*, 2001; **293**: 1119-1122; (c) Q. Sun, L. Dai, X. Zhou, L. Li and Q. Li, *Appl. Phys. Lett.*, 2007; **91**: 253505; (d) S-S. Sun, N. S. Sariciftci *Organic Photovoltaics: Mechanisms, Materials, and Devices*, Taylor & Francis, Boca Raton, FL, 2005.
  16. (a) F. Lelj, G. Morelli, G. Ricciardi, A. Roviello and A. Sirigu. *Liq. Cryst.*, 1992, **12**, 6, 941-960; (b) S. Belviso, G. Ricciardi and F. Lelj, *J. Mater. Chem*, 2000, **10**, 297-304.
  17. (a) A. M. Giroud-Godquin and P. M. Maitlis., *Angew. Chem., Int. Ed. Engl.*, 1991, **30**, 375-402; (b) M. Sato, A. Takeuchi, T. Yamada, H. Hoshi, K. Ishikawa, T. Mori and H. Takezoe, *Phys. Rev. E*, 1997, **56**, R6264-R6266; (c) G. Serrano, *Metallomesogens*, VCH, Berlin, 1995; (d) S. Chandrasekhar, *Liquid Crystals*, Cambridge University Press, Cambridge, UK, 2nd Edn., 1992; (e) D. Demus, J. Goodby, G. W. Gray, H. W. Spiess and V. Vill, *Handbook of Liquid Crystals*, Wiley-VCH, New York, 1998, vol. 2B.

- 
18. S. Belviso, M. Amati, M. De Bonis and F. Lejl, *Mol. Cryst. Liq. Cryst.*, 2008, **481**, 56–72.
19. J.-P. Corbet and G. Mignani, *Chem. Rev.*, 2006, **106**, 2651–2710.
20. N. Miyaura and A. Suzuki, *Chem. Rev.*, 1995, **95**, 2457–2483.
21. R. Gauler, R. Keuper, A. Winter and N. Risch, *Arkivoc.*, 2004, **8**, 48-56.
22. K. Sonogashira, Y. Tohda and N. Hagihara, *Tetrahedron Lett.*, 1975, 4467-4470.
23. W. M. Sharman and J. E. Van Lier, *J. Porphyrins Phthalocyanines*, 2000, **4**, 441–453.
24. C. M. Muzzi, C. J. Medforth, L. Voss, M. Cancilla, C. Lebrilla, J. –G. Ma, J. A. Shelnut and K. M. Smith, *Tetrahedron Lett.*, 1999, **40**, 6159–6162.
25. (a) B. Vaz, R. Alvarez, M. Nieto, A. I. Paniello and A. R. de Lera, *Tetrahedron Lett.*, 2001, **42**, 7409-7412; (b) J.-P. Tremblay-Morin, H. Ali and J. E. van Lier *Tetrahedron Lett.* 2006, **47**, 3043–3046.
26. (a) L. A. Bottomley and W. H. Chiou, *J. Electroanal. Chem.*, 1986, **198**, 331-346; (b) E. A. Ough, K. A. M. Creber and M. J. Stillman, *Inorg. Chim. Acta*, 1996, **246**, 361-369.
27. The number of exchanged electrons in each of these redox processes is also confirmed by analyzing the width of the peaks at half height in the corresponding differential small pulse amplitude voltammograms. Considering that in our pulse voltammograms obtained using a pulse amplitude of 50 mV, the measured values of the peak half widths were greater than 90.4 mV, a one–electron reduction processes has to be associated with all the studied compounds. See: E. P. Perry and R. A. Osteryoung, *Anal. Chem.*, 1965, **37**,1634-1637.
28. (a) M. J. Fuchter, L. S. Beall, S. M. Baum, A. G. Montalban, E. G. Sakellariou, N. S. Mani, T. Miller, B. J. Vesper, A. J. P. White, D. J. Williams, A. G. M. Barrett and B. M. Hoffman, *Tetrahedron*, 2005, **61**, 6115-6130; (b) M. J. Fuchter, B. J. Vesper, K. A. Murphy, H. A. Collins, D. Phillips, A. G. M. Barrett and B. M. Hoffman, *J. Org. Chem.*, 2005, **70**, 2793-2802.

- 
29. (a) M. -C. Kuo, L. -A. Li, W. -N. Yen, S. -S. Lo, C. -W. Lee and C. -Y. Yeh, *Dalton Trans.*, 2007, 1433-1439; (b) H. L. Anderson, A. P. Wylie and K. Prout, *J. Chem. Soc., Perkin Trans. I*, 1998, **1**, 1607-1611.
30. H. Xu, R. Chen, Q. Sun, W. Lai, Q. Su, W. Huang and X. Liu, *Chem. Soc. Rev.*, 2014, **43**, 3207-3812.
31. (a) M. Gouterman, *J. Molecular Spectroscopy*, 1961, **6**, 138-163; (b) M. Gouterman, D. Holten and E. Lieberman, *Chem. Phys.*, 1977, **25**, 139-153; (c) M. Gouterman, in *The Porphyrins*, D. Dolphin Ed.; Academic Press: New York, 1978, Vol. 3.
32. I. Infante and F. Lelj, *J. Chem. Theor. Comput.*, 2007, **3**, 838-851.
33. P. A. Stuzhin, *J. Porphyrins Phthalocyanines*, 1999, **3**, 500-513 and references therein.
34. (a) H. L. Anderson, S. J. Martin and D. D. C. Bradley, *Angew. Chem., Int. Ed. Engl.*, 1994, **33**, 655-657; (b) S. J. Martin, H. L. Anderson and D. D. C. Bradley, *Adv. Mater. Optics Electronics*, 1994, **4**, 277-283; (c) S. J. Martin, D. D. C. Bradley and H. L. Anderson. *Mol. Cryst. Liq. Cryst.*, 1994, **256**, 649-655; (d) G. E. O'Keefe, G. J. Denton, E. J. Harvey, R. T. Philips, R. H. Friend and H. L. Anderson, *J. Chem. Phys.*, 1996, **104**, 805-811; (e) D. Beljonne, G. E. O'Keefe, P. J. Hamer, R. H. Friend, H. L. Anderson and J. L. Brédas, *J. Chem. Phys.*, 1997, **106**, 9439-9460 ; (f) S. M. LeCours, S. G. DiMugno and M. J. Therien, *J. Am. Chem. Soc.*, 1996, **118**, 11854-11864; (g) F. Z. Henari, W. J. Blau, L. R. Milgrom, G. Yahioglu, D. Phillips and J. A. Lacey, *Chem. Phys. Lett.*, 1997, **267**, 229-233.
35. S. Laschat, A. Baro, N. Steinke, F. Giesselmann, C. Hagele, G. Scalia, R. Judele, E. Kapasina, S. Sauer, A. Schreivogel and M. Tosoni, *Angew. Chem., Int. Ed. Engl.*, 2007, **46**, 4832-4887.
36. (a) J. Barberà, O. A. Rakitin, M. B. Ros and T. Torroba, *Angew. Chem., Int. Ed. Engl.*, 1998, **37**, 296-299; (b) F. Nekelson, H. Monobe and Y. Shimizu, *Chem. Comm.*, 2006, 3874-3876; (c) M. Suarez, J. M. Lehn, S. C. Zimmerman, A. Skoulios and B. Heinrich,

- 
- J. Am. Chem. Soc.*, 1998, **120**, 9526-9532; (d) C. Desdrade, P. Foucher, H. Gasparoux, N. H. Tinh, A. M. Levelut and J. Malthete, *Mol. Cryst. Liq. Cryst.*, 1984, **106**, 121-146.
37. H. Zheng, C. K. Lai and T. M. Swager, *Chem. Mater.* 1995, **7**, 2067-2077.
38. (a) G. Ricciardi, A. Bavoso, A. Bencini, A. Rosa, F. Lejl and F. Bonosi, *J. Chem. Soc., Dalton Trans.*, 1996, 2799-2807; (b) N. Kobayashi, S. Nakajima and T. Osa, *Chem. Lett.*, 1992, **12**, 2415-2418 and references therein; (c) G. Ricciardi, A. Rosa, I. Ciofini and A. Bencini, *Inorg. Chem.*, 1999, **38**, 1422-1431; (d) G. Ricciardi, A. Bencini, A. Bavoso, A. Rosa and F. Lejl, *J. Chem. Soc., Dalton Trans.*, 1996, 3243-3249.
39. (a) D. M. Knawby and T. M. Swager. *Chem. Mater.*, 1997, 535-538; (b) J. Martinsen, J. L. Stanton, R. L. Greene, J. Tanaka, B. M. Hoffman and J. Ibers. *J. Am. Chem. Soc.*, 1985, **107**, 6915-6920; (c) F. Wudl. *Acc. Chem. Res.*, 1984, **17**, 227-232.
40. P. L. Cristinziano and F. Lejl. *J. Chem. Phys.*, 2007, **127**, 134506-134513.
41. S. Chandrasekhar and G. S. Ranganath, *Rep. Prog. Phys.* 1990, **53**, 57-84.
42. A. J. Bard and L. R. Faulkner, *Electrochemical Methods, Fundamentals and Applications*, John Wiley & Sons, New York, 1980.
43. Gaussian 09, Revision C.01, M. J. Frisch, G. W. Trucks, H. B. Schlegel, G. E. Scuseria, M. A. Robb, J. R. Cheeseman, G. Scalmani, V. Barone, B. Mennucci, G. A. Petersson, H. Nakatsuji, M. Caricato, X. Li, H. P. Hratchian, A. F. Izmaylov, J. Bloino, G. Zheng, J. L. Sonnenberg, M. Hada, M. Ehara, K. Toyota, R. Fukuda, J. Hasegawa, M. Ishida, T. Nakajima, Y. Honda, O. Kitao, H. Nakai, T. Vreven, J. A. Montgomery, Jr., J. E. Peralta, F. Ogliaro, M. Bearpark, J. J. Heyd, E. Brothers, K. N. Kudin, V. N. Staroverov, T. Keith, R. Kobayashi, J. Normand, K. Raghavachari, A. Rendell, J. C. Burant, S. S. Iyengar, J. Tomasi, M. Cossi, N. Rega, J. M. Millam, M. Klene, J. E. Knox, J. B. Cross, V. Bakken, C. Adamo, J. Jaramillo, R. Gomperts, R. E. Stratmann, O. Yazyev, A. J. Austin, R. Cammi, C. Pomelli, J. W. Ochterski, R. L. Martin, K. Morokuma, V. G. Zakrzewski, G. A. Voth, P. Salvador, J. J. Dannenberg, S. Dapprich, A. D. Daniels, O. Farkas, J. B. Foresman, J. V. Ortiz, J. Cioslowski, and D. J. Fox, Gaussian, Inc., Wallingford CT, 2010

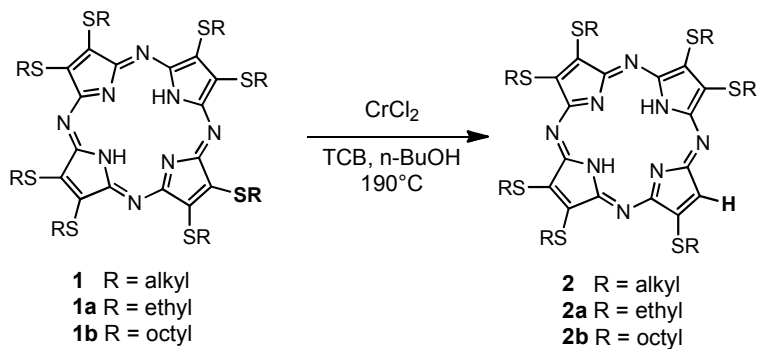
- 
44. A. D. Becke, *J. Chem. Phys.* 1993, **98**, 5648-5652.
45. (a) J. S. Binkley, J. A. Pople and W. J. Hehre, *J. Am. Chem. Soc.*, 1980, **102**, 939-947;  
(b) M. S. Gordon, J. S. Binkley, J. A. Pople, W. J. Pietro and W. J. Hehre, *J. Am. Chem. Soc.*, 1982, **104**, 2797-2803.
46. (a) Casida, M. *Time dependent density functional response theory for molecules*, in “Recent advances in Density Functional Methods”; D. P. Chong, Ed.; World Scientific: Singapore, 1995; vol. 1; p. 155; (b) M. E. Casida, C. Jamorski, K. C. Casida and D. R. Salahub, *J. Chem. Phys.* 1998, **108**, 4439-4449.
47. R. E. Stratmann, G. E. Scuseria and M. J. Frisch, *J. Chem. Phys.*, 1998, **109**, 8218-8224.
48. Y. Zhao and D. G. Truhlar, *Theor. Chem. Acc.*, 2008, **120**, 215-241.
49. J. Tomasi, B. Mennucci and R. Cammi, *Chem. Rev.*, 2005, **105**, 2999-3093.
50. G. Schaftenaar and J. H. Noordik, *J. Comput.-Aided Mol. Design*, 2000, **14**, 123-134.

**Table 1.** Summary of the peak potentials  $E_{1/2}$  ( $\Delta E_p = |E_a - E_c|$ ) (Volts vs Fc/Fc<sup>+</sup>) for the new synthesised compounds.<sup>a</sup>

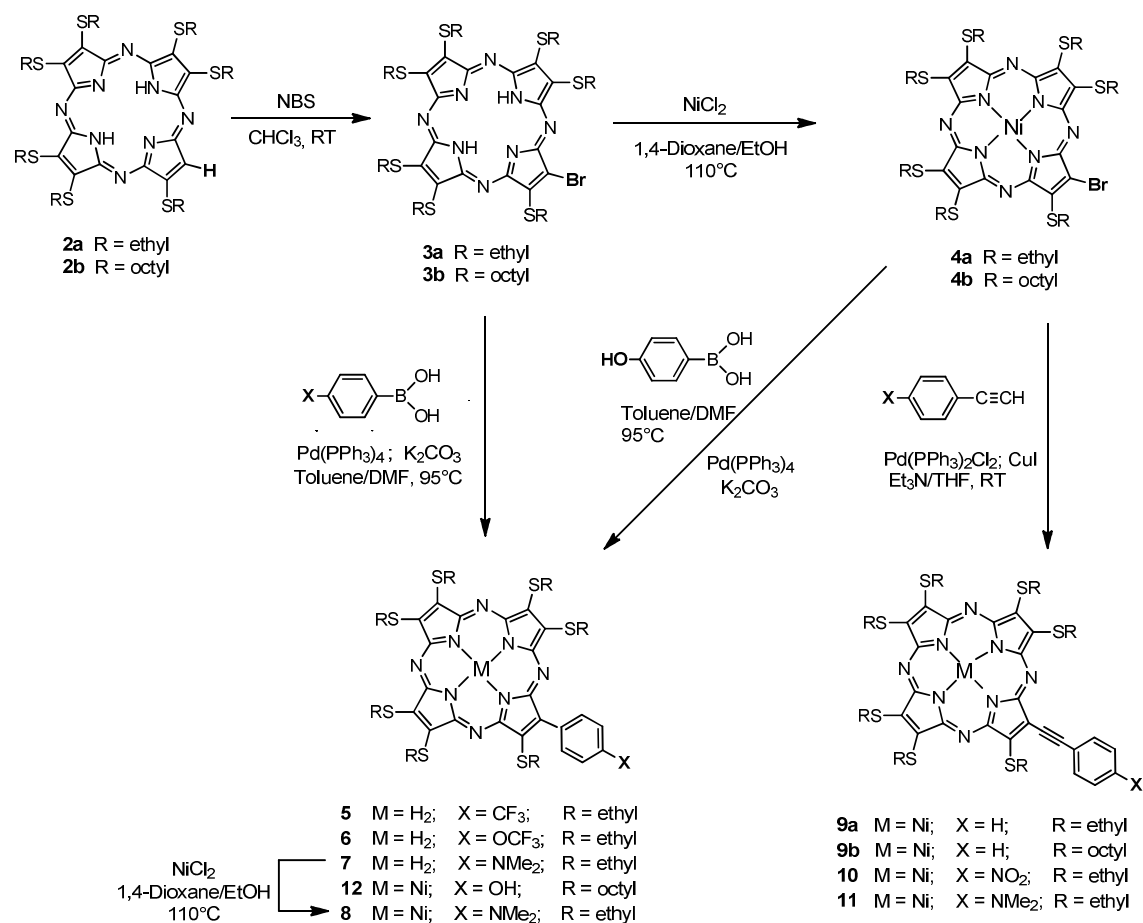
Compound	Technique	Oxidation	Reduction		HOMO		LUMO	
			I	II	Exptl <sup>d</sup>	Compt <sup>b</sup>	Exptl <sup>d</sup>	Compt <sup>b</sup>
3a	(CV)	0.668	-0.869 (0.078)	-1.193 (0.078)	-5.468	-6.438	-3.931	-2.474
	<sup>d</sup> I <sub>pa</sub> /I <sub>pc</sub>	1.05	1.02	0.93		-5.627 (sol)		-3.869 (sol)
	(DPV) <i>red</i>	0.665	-0.865	-1.199	-5.465		-3.935	
	(DPV) <i>ox</i>	0.667	-0.838	-1.170	-5.467		-3.962	
4a	(CV)		-1.004 (0.098)	-1.360 (0.098)		-6.469	-3.796	-2.308
	I <sub>pa</sub> /I <sub>pc</sub>		1.35	0.83		-5.657 (sol)		-3.700 (sol)
	(DPV) <i>red</i>	0.759	-0.957	-1.333	-5.559		-3.843	
	(DPV) <i>ox</i>	0.894	-0.986	-1.360	-5.694		-3.814	
5	(CV)	0.655 (0.110)	-0.874 (0.084)	-1.192 (0.080)	-5.455	-6.443	-3.926	-2.423
	I <sub>pa</sub> /I <sub>pc</sub>	0.20	0.96	0.81		-5.609 (sol)		-3.751 (sol)
	(DPV) <i>red</i>	0.718	-0.870	-1.200	-5.518		-3.930	
	(DPV) <i>ox</i>	0.662	-0.855	-1.198	-5.462		-3.945	
6	(CV)	0.678 (0.090)	-0.877 (0.076)	-1.198 (0.078)	-5.478	-6.464	-3.923	-2.466
	I <sub>pa</sub> /I <sub>pc</sub>	0.34	0.80	0.70		-5.639 (sol)		-3.808 (sol)
	(DPV) <i>red</i>	0.721	-0.876	-1.208	-5.521		-3.924	
	(DPV) <i>ox</i>	0.661	-0.887	-1.216	-5.461		-3.913	
7	(CV)	0.374 (0.035)	-0.913 (0.084)	-1.246 (0.086)	-5.174	-5.930	-3.887	-2.260
	I <sub>pa</sub> /I <sub>pc</sub>	1.07	1.07	0.73		-5.187 (sol)		-3.694 (sol)
	(DPV) <i>red</i>	0.378	-0.902	-1.234	-5.178		-3.898	
	(DPV) <i>ox</i>	0.346	-0.924	-1.260	-5.146		-3.876	
8	(CV)	0.357 (0.082)	-1.056 (0.092)	-1.418 (0.076)	-5.157	-5.976	-3.744	-2.197
	I <sub>pa</sub> /I <sub>pc</sub>	0.69	1.06	0.98		-5.236 (sol)		-3.588 (sol)
	(DPV) <i>red</i>	0.360	-1.050	-1.423	-5.160		-3.750	
	(DPV) <i>ox</i>	0.358	-1.047	-1.414	-5.158		-3.753	
9a	(CV)	0.676 (E <sub>p</sub> )	-0.981 (0.110)	-1.278 (0.040)	-5.476	-6.340	-3.819	-2.301
	I <sub>pa</sub> /I <sub>pc</sub>		1.22	0.68		-5.605 (sol)		-3.670 (sol)
	(DPV) <i>red</i>	0.682	-0.972	-1.238	-5.482		-3.828	
	(DPV) <i>ox</i>	0.602	-0.970	-1.238	-5.402		-3.830	
9b	(CV)	0.757 (E <sub>p</sub> )	-1.068	-1.384	-5.557	-6.340	-3.732	-2.301
	I <sub>pa</sub> /I <sub>pc</sub>		1.16	0.70		-5.605 (sol)		-3.670 (sol)
	(DPV) <i>red</i>	0.720	-1.062	-1.382	-5.520		-3.738	
	(DPV) <i>ox</i>	0.642	-1.046	-1.384	-5.442		-3.754	
10	(CV)	0.750 (E <sub>p</sub> )	-0.923 (0.074)	-1.216 (0.096)	-5.550	-6.525	-3.877	-2.586
	I <sub>pa</sub> /I <sub>pc</sub>		0.78	0.55		-5.667 (sol)		-3.813 (sol)
	(DPV) <i>red</i>	0.750	-0.914	-1.244	-5.550		3.886	
	(DPV) <i>ox</i>	0.686	-0.898	-1.212	-5.486		-3.902	
11	(CV)	0.375 (E <sub>p</sub> )	-1.008 (0.114)	-1.344 (0.122)	-5.175	-5.871	-3.792	-2.179
	I <sub>pa</sub> /I <sub>pc</sub>		1.30	0.83		-5.169 (sol)		-3.607 (sol)
	(DPV) <i>red</i>	0.318	-1.016	-1.356	-5.118		-3.784	
	(DPV) <i>ox</i>	0.302	-0.986	-1.342	-5.102		-3.814	
12	(CV)	0.662 (E <sub>p</sub> )	-1.028 (0.112)	-1.421 (0.102)	-5.462	-6.301	-3.772	-2.304
	I <sub>pa</sub> /I <sub>pc</sub>		0.71	0.56		-5.572 (sol)		-3.680 (sol)
	(DPV) <i>red</i>	0.766	-1.024	-1.436	-5.566		-3.776	
	(DPV) <i>ox</i>	0.732	-1.028	-1.458	-5.532		-3.772	

<sup>a</sup> Measured in CH<sub>2</sub>Cl<sub>2</sub> solution 10<sup>-3</sup> M in compound at a glassy carbon working electrode. **DPV**: Scan rate of 5 Vs<sup>-1</sup>; Pulse Height of 50 mV, Pulse Width 50 ms. **CV**: scan rate of 200 mVs<sup>-1</sup>. <sup>b</sup> Values, in eV, referred to first oxidation and first reduction, and calculated assuming the energy level for ferrocene at -4.8 eV [E. P. Pery and R. A. Osteryoung, *Anal. Chem.*, 1965, 1634]. <sup>c</sup> in-vacuum and PCM-based computations as described in Experimental section. <sup>d</sup> I<sub>pa</sub>/I<sub>pc</sub> for the reduction, I<sub>pc</sub>/I<sub>pa</sub> for the oxidation processes.

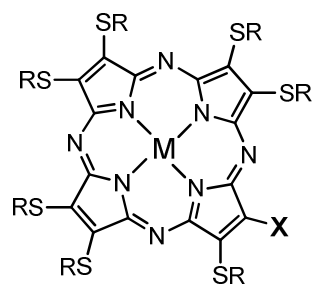
## Figures and Schemes



Scheme 1



Scheme 2



R = octyl

- 2c** M = Ni, X = H  
**4b** M = Ni, X = Br  
**9b** M = Ni, X = C≡CPh  
**12** M = Ni, X = 4-OHPh  
**13** M = H<sub>2</sub>, X = Ph  
**14** M = Ni, X = Ph  
**15** M = Ni, X = 4-NMe<sub>2</sub>Ph

Chart

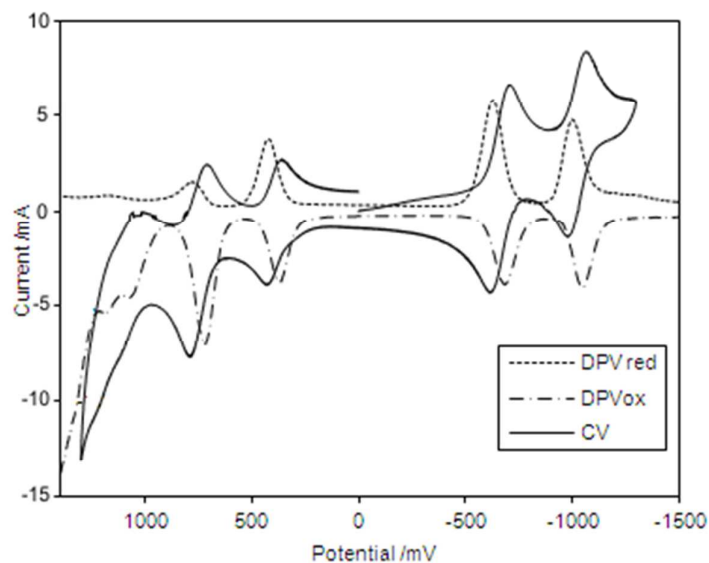


**Figure 1.** Cyclic voltammogram and differential pulse voltammograms of **8** in  $\text{CH}_2\text{Cl}_2$ .

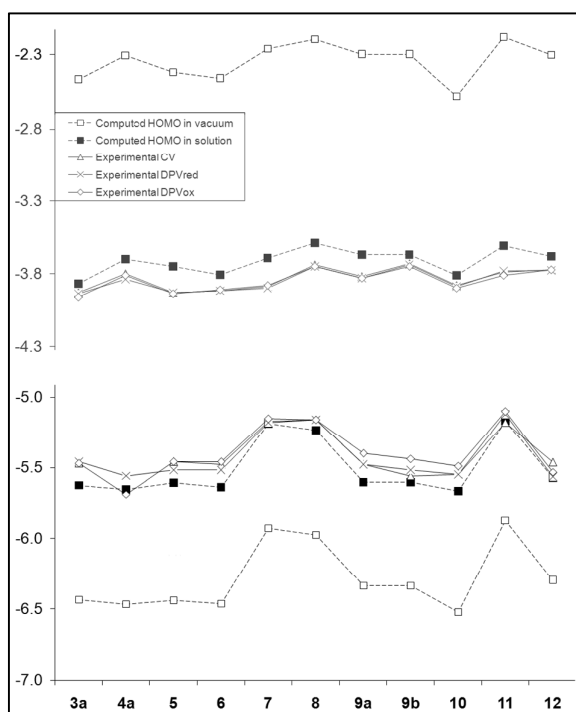


**Figure 2.** Comparison among experimental and computational HOMO (bottom part of the energy axis) and LUMO (top part) energies. Table 1 lists the reported values.

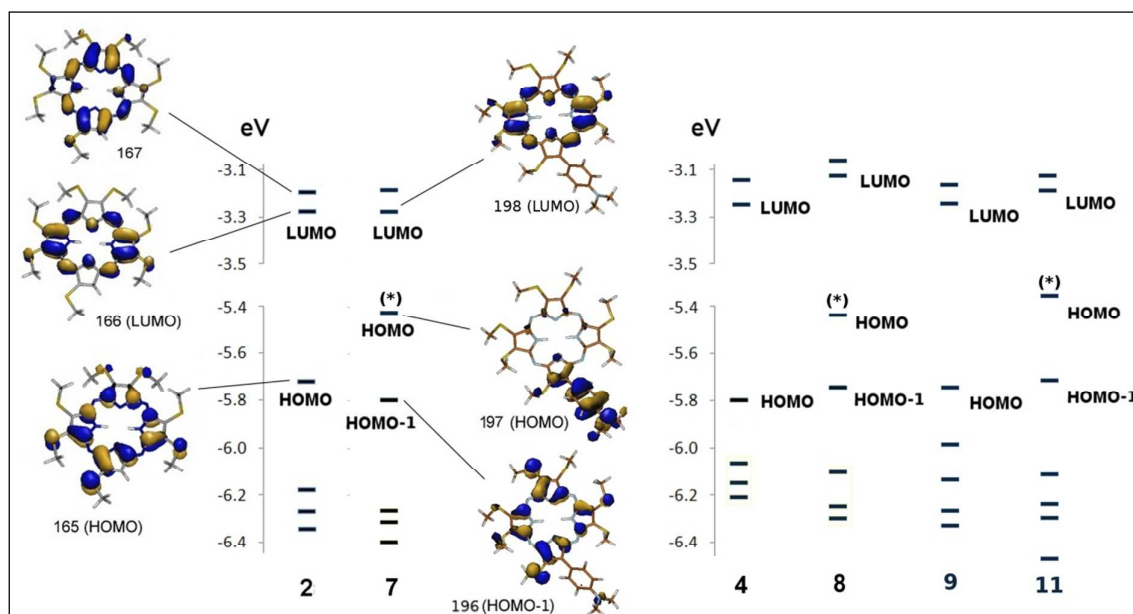


**Figure 3.** Kohn-Sham orbitals energies of selected compounds and graphical representations of **2** and **7** Kohn-Sham orbitals close to the HOMO and LUMO. In the energy levels scheme, the asterisk labels the orbitals which are localized on the asymmetric substituent (similar to orbital 197, HOMO, in **7**). All the other levels are associated to macrocycle-localized orbitals.

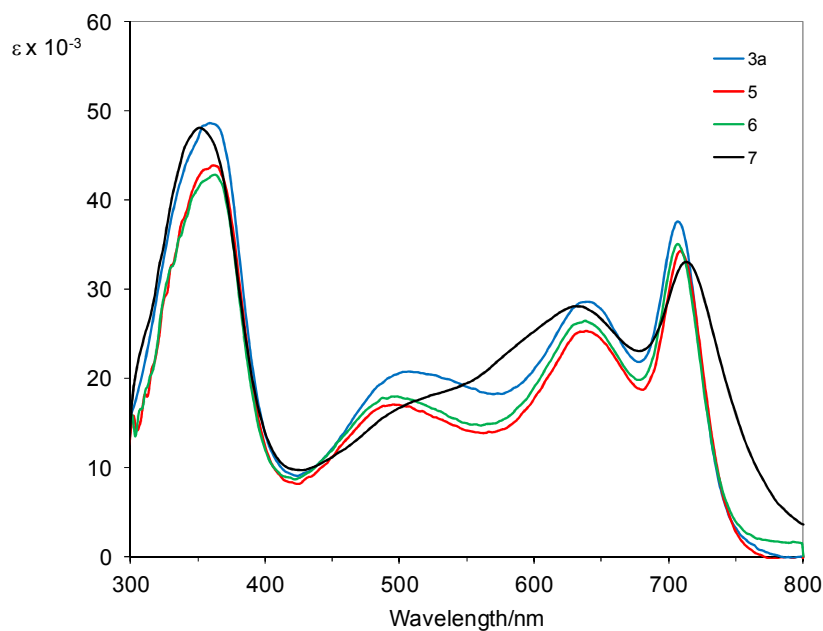


**Figure 4.** UV spectra in  $\text{CH}_2\text{Cl}_2$  of “free base” porphyrazines **3a**, **5-7**.

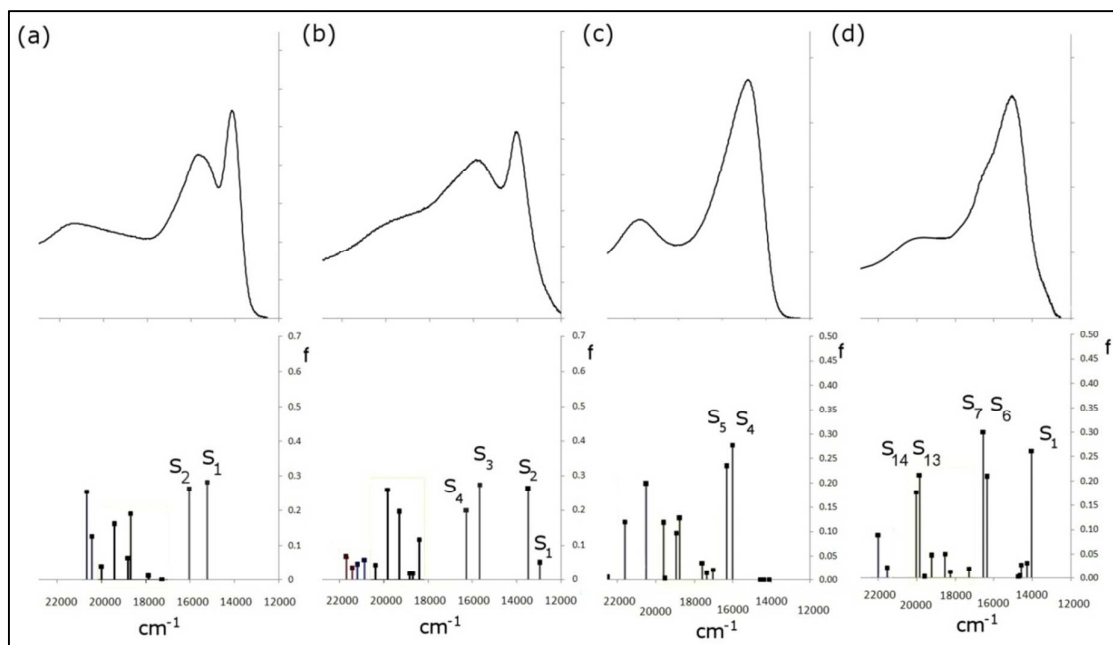


**Figure 5.** Experimental UV-Vis spectra of **2a** (a), **7** (b), **4a** (c) and **8** (d) in the low energy part of the absorption spectra (Q band and extra band) recorded in  $\text{CH}_2\text{Cl}_2$  solution. Computational TDDFT-based results are reported below the experimental one for comparison. The experimental absorbance is in arbitrary units, computed oscillator strengths are sketched as vertical rods.

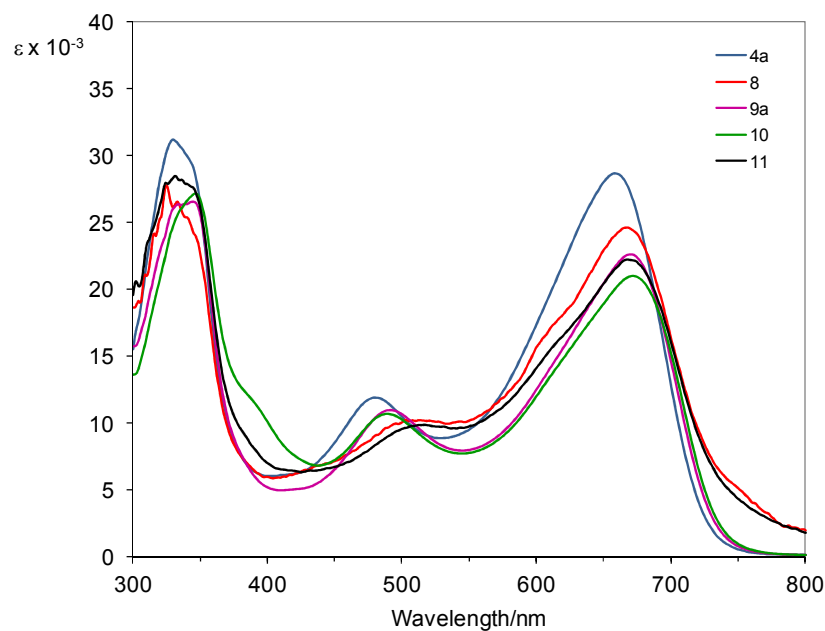


**Figure 6.** UV spectra in  $\text{CH}_2\text{Cl}_2$  of Ni-complexes porphyrazines **4a**, **8**, **9a**, **10**, **11**.

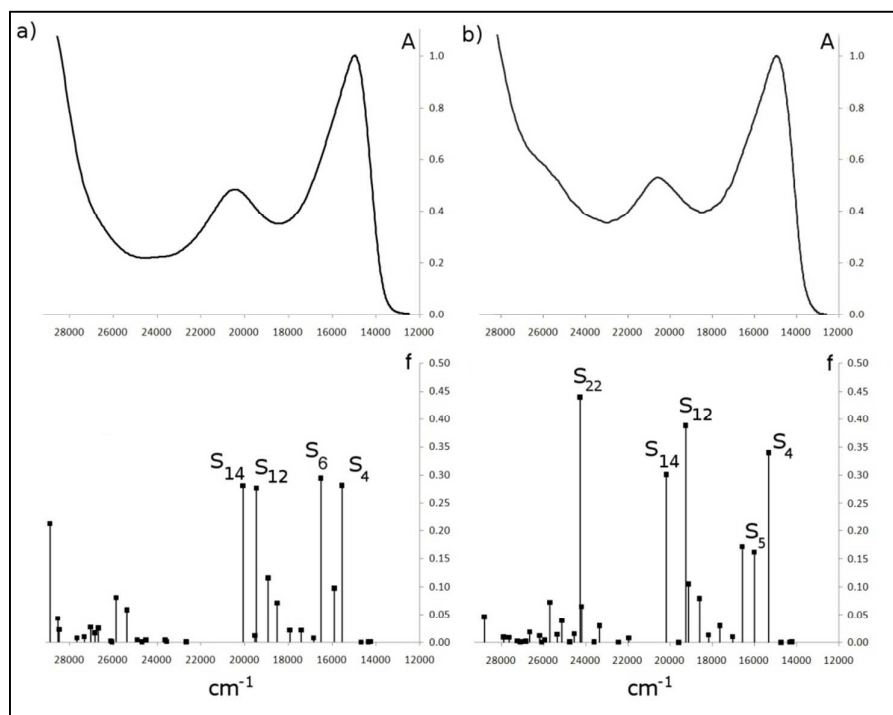


**Figure 7.** UV-Vis spectra of **9a** (a) and **10** (b) recorded in  $\text{CH}_2\text{Cl}_2$  solution. For a better comparison the experimental spectra were normalized by using the Q band maximum and computational TDDFT-based results are reported below the experimental one. The experimental absorbance is in arbitrary units, computed oscillator strengths are sketched as vertical rods.

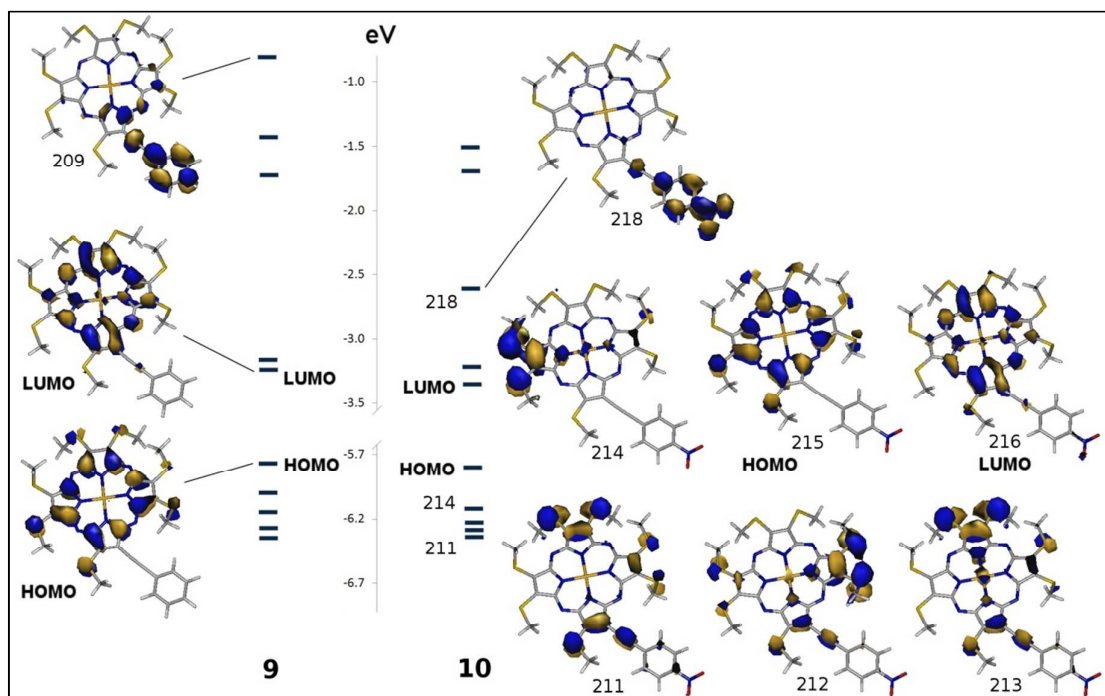


**Figure 8.** Kohn-Sham orbitals energy levels of **9** and **10** and graphical representations of some more relevant orbitals. Due to the electron withdrawing action of the  $\text{NO}_2$  group, the **9** LUMO+4 (orbital 209) is lowered in energy in **10** and becomes the LUMO+2 (orbital 218).

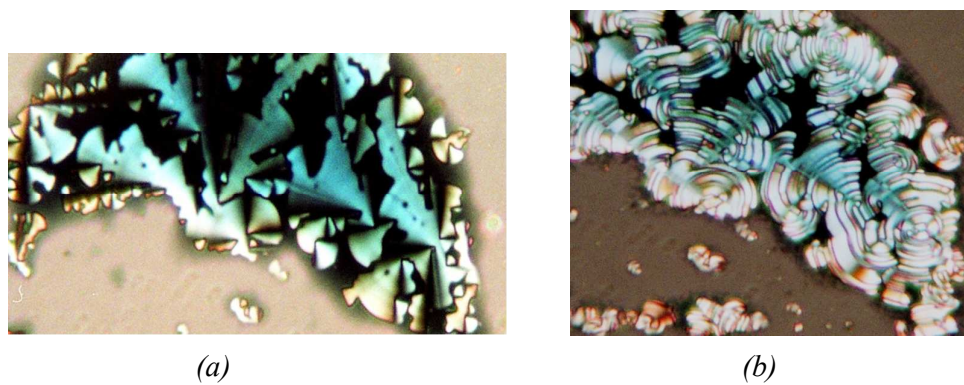


**Figure 9.** Liquid-crystalline textures shown by **12** on cooling the liquid phase at 83.1°C (*a*) and at 63.4 °C (*b*). Crossed polarizers microscope 32X.

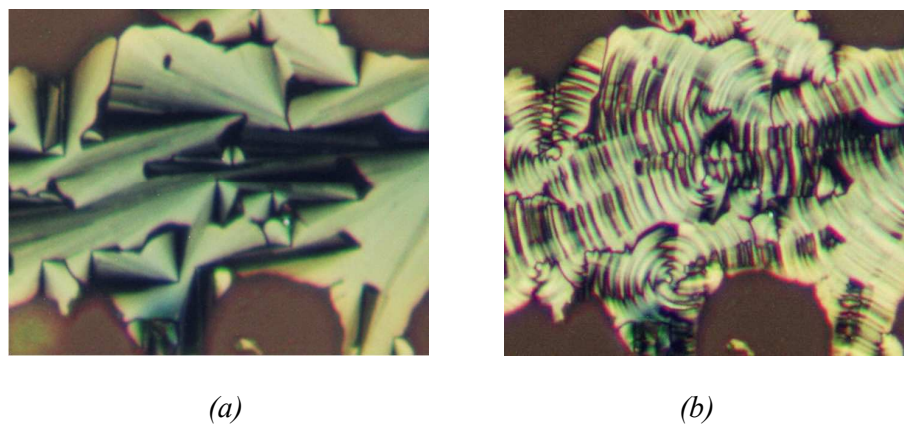


**Figure 10.** Liquid-crystalline textures shown by **9b** on cooling the liquid phase at 110.0°C (*a*) and at 25.0 °C (*b*). Crossed polarizers microscope 32X.

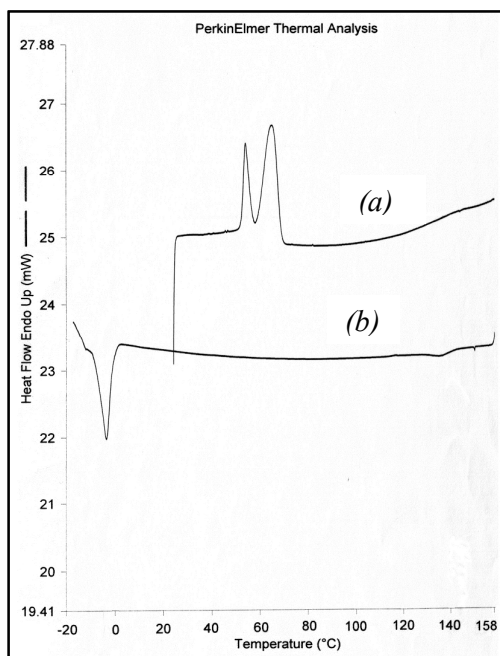


**Figure 11.** DSC thermograms of compound **9b**: (a) First heating curve of a solution crystallized sample with no thermal treatment; (b) first cooling curve. Scan rate 5 °C/ min.